Design and Testing of a Variable Stiffness Transverse Plane Adaptor for Use in a Lower Limb Prosthesis

Corey Pew

A thesis submitted in

partial fulfillment of the requirements

for the degree of

Master of Science in Mechanical Engineering

University of Washington

2014

Committee:

Glenn Klute, PhD

Randal Ching, PhD

Santosh Devasia, PhD

Program Authorized to Offer Degree:

Mechanical Engineering

University of Washington

Abstract

Design and Testing of a Variable Stiffness Transverse Plane Adaptor for Use in a Lower Limb Prosthesis

Corey Pew

Chair of the Supervisory Committee:

Glenn Klute, Ph.D.

Affiliate Associate Professor, Department of Mechanical Engineering

Background

The goal of a lower limb prosthesis is to restore the abilities of the intact limb for an amputee. Daily ambulation includes many maneuvers such as turning, pivoting, and uncertain terrain, all of which require a component of transverse plane mobility. It has been shown that the addition of a transverse plane adaptor can help to decrease soft tissue damage, increase mobility, and help reduce the risk of falls in amputees. However, currently available transverse plane adaptors only allow for a single stiffness setting and do not allow for variation to accommodate the maneuvers of everyday ambulation. The aim of this research was to design, build, and test a prototype lower limb prosthetic adaptor that is capable of variable stiffness in the transverse plane. The device will be used to better understand the role transverse stiffness plays in varying daily ambulation activities such as walking and turning.

Design

A variable stiffness torsion device (VSTA) was designed, and built and is capable of controlling stiffness in the transverse plane of a lower limb prosthesis. Design criteria were established to determine structural and functional requirements for the VSTA. A custom spring was designed with a rate of 0.33 Nm/° allowing for VSTA settings between 0.10-1.17 Nm/°, and includes a locked infinitely stiff setting. Refinement of the design was then conducted using a mathematical model, finite element analysis (FEA), and analysis of VSTA kinematics. Following design completion, a prototype was built and tested.

Mechanical Testing

Mechanical bench testing was performed to determine the physical capabilities of the VSTA. The VSTA is actually capable of infinite stiffness variation between 0.12-0.91 Nm/°. Initial designs accounted for the internal spring to be capable of 90° of deflection which would have allowed for infinite stiffness variation between the minimum and infinitely stiff, however, internal spring stresses limited spring deflection to 57°, resulting in the limited range of the VSTA. The bench testing showed that the VSTA as designed and manufactured would be suitable for human subjects testing.

Controller Testing

A proportional-integral-derivative (PID) controller, provided by the motor manufacturer, was used to control step inputs of the spring carrier to adjust the stiffness of the VSTA. The controller, using a 16 volt supply, could accurately perform step inputs, but could not meet rate of performance design goals. When supply voltage was brought up to the ideal 24 volts the controller was able to meet the rate goals of the VSTA, however, over power faults occurred resulting in incomplete step controls. Use of a different control module that would allow for the full 24 volt supply to the motor and with consideration of the reduced functional range of the VSTA it is estimated that the controller would meet all design goals.

Future Work

Structurally the VSTA needs to be improved beyond the factor of safety of one to provide a more robust solution. Mechanical improvements include increasing VSTA ability to apply and sustain higher

stiffness settings without being limited by overstress of the spring. It would also be beneficial to test the VSTA for use as an active stiffness generator, modulating stiffness while under load. Additionally, the controller could be developed to better optimize the gains, and possibly increase speed and performance of the system. Lastly, human subjects testing should be conducted to better evaluate the VSTA's ability to function in a real setting, as well as to better understand the role of transverse plane stiffness during ambulation.

TABLE OF CONTENTS

List of Figures

List of Tables

1 Background

Amputation is a serious life altering event, but with the help of modern prostheses an amputee can continue a normal active life. In 2005 there were over one million people in the US living with lower limb amputation, and by the year 2050, that number is projected to rise to almost 2.5 million [1]. Of these lower limb amputees, 58% were under the age of 65, and 20% under the age of 44. This implies that many amputees live a significant portion of their lives with their condition. The natural human leg allows for movement in multiple planes of motion, providing numerous degrees of freedom. When the limb is removed and replaced with a prosthesis, only a few of those degrees of freedom are restored. Much of research and new device design focuses on straight line walking, with particular emphasis on the sagittal plane. This approach tends to ignore turning and other complex maneuvers requiring motion in the transverse plane [2,3]. Preliminary research, described in the following paragraphs, suggests that a device that allows for variable stiffness in the transverse plane could help reduce soft tissue damage at the socket interface, improve mobility, as well as help prevent falls.

1.1 Soft Tissue Damage

The outer soft tissues of the lower leg are not evolved to transmit the high loads of ambulation. Because of this, the residual limbs of amputees have been shown to have chronic dermal ailments such as abrasions, cysts, and ulcers [4]. The high stress of the prosthesis can also cause decreases in venous return, and reduce lymphatic drainage, which can be extremely detrimental to amputees with compromised vascular systems (80% of lower limb amputees) [1], [4–6]. While exoskeleton style prostheses will always exhibit these issues to some degree, a torsion adaptor can be used to reduce peak shear stresses that contribute to them [8]–[10]. A torsion adaptor could be of benefit for a lower limb amputee who exhibits soft tissue damage from high stresses, or vascular compromise.

1.2 Amputee Mobility

Mobility is a main concern for the amputee, and while research into straight line walking is acceptable for initial development, it has been shown that turns constitute a considerable amount of a person's daily locomotion [11]. Lamoureux and Radcliff indicated as early as 1977 that the addition of a torsion adaptor could "Improve freedom of movement when changing direction of motion, working at a bench or computer, and in sports activities" [8]. It has also been observed that a torsion adaptor can improve walking gait, and the negotiation of rough terrain, all while reducing energy consumption [12], [13]. These studies can be seen to imply that the use of a torsion adaptor leads to improved mobility which can lead to amputees being more independent, healthier, and less likely to need support services over the course of their life.

1.3 Amputee Falling

Falls are a serious issue for the amputee; 52% of all amputees have experienced a fall in a single year, and 49% exhibit a fear of falling that can lead to avoidance of activities [14]. The fear of falling reduces activity levels that can generally help improve muscle endurance, strength, and flexibility, and so activity avoidance can be related to further loss of balance and coordination [14]. Turning has been shown to be less stable than straight line walking [15] and the inclusion of a torsion adaptor may help increase stability in turns for amputees [16]. The inclusion of a torsion adaptor, particularly one with variable stiffness characteristics to help simulate the torsion of intact ankle during turns, has been theorized to be a benefit to the amputee when negotiating a turn [12], [17]. A torsion adaptor could help to increase stability in a turn which could lead to fewer falls, and a decreased avoidance of daily activities that limit amputee mobility.

1.4 Variable Stiffness Torsion

While the need for a torsion adaptor has been shown, current adaptors on the market only allow for a single setting for torsional stiffness that is non-adjustable by the user [18]. This means that the adaptor is incapable of adapting itself to the different conditions the user might face such as turning, pivoting, stairs, ramps, or rough terrain. It has also been shown that the stiffness of joints, such as the ankle, naturally have a variable stiffness that changes based on gait dynamics [19], further supporting the need for a variable stiffness torsion adapter.

It is the point of this project to design and build a prototype variable stiffness torsion adaptor that can be used to better understand how transverse plane stiffness can be adapted to various modes of ambulation, and what stiffness levels might be optimal for those modes. Future work will use this prototype to determine if variable stiffness in the transverse plane of a lower limb prosthesis is of benefit to the amputee.

2 Design

To improve the mobility of lower limb amputees who perform a variety of ambulatory tasks and might benefit from variable torsional stiffness, a novel prosthesis that fits in the prosthetic pylon was designed. This section outlines the design evolution of the variable stiffness torsion adaptor (VSTA). The design steps included concept generation facilitated by a literature search of current devices that could be adapted to fit the needs of this project. Next, design criteria were generated based on structural and functional needs of the VSTA. A description of the device as originally designed is outlined followed by the methods used to derive the design. Lastly, design modifications that arose during fabrication and bench testing are presented.

2.1 Concept Investigation

A review of research in the fields of prosthetics, robotics, rehabilitation, and other varied disciplines yielded four different concepts that could be adapted as a variable stiffness torsion adaptor. The concepts were evaluated based on five different criteria: 1) size and mass, 2) functionality, 3) power consumption, 4) failure scenario, and 5) cost. Each category was given a score between one and five, where five was considered best and each category was weighted to emphasize relevance to the final design goals. The most viable concept (highest score) was then further developed into the VSTA.

The first category, size and mass, evaluates how well the design might fit onto an existing prosthesis and how heavy it might be. This was given a weight of one because it is relatively important, but can generally be improved post-prototype with refined design criteria and advanced materials. Functionality, the most important aspect, was appraised with a weighting of two. This was an evaluation of how well the concept would be able to actively vary the stiffness when used in a lower limb prosthesis. Power consumption was given a weighting of one and a half. This is an estimation of how much power the electric motor might consume, affecting motor selection and battery size, influencing weight, cost, and function. Failure scenario had a weight of one. This is an evaluation of how the device would operate if there was a failure of the electronics, motor, or variability device. This was deemed relatively important because at some point most devices experience failure that can adversely affect the user, however, these failure conditions can be addressed in later design iterations if necessary. Lastly, cost was evaluated at with a weighting of one-half. While cost is always a driving factor in any device design, medical devices tend to look at cost secondary to benefit and function, and can also be designed around in later iterations. The following paragraphs go into more detail for each design and describe the subsequent ratings with Table 1 summarizing the scores.

2.1.1 Variable Pivot

The first possible design is one similar to the AwAS-II described by Jafari et. al. [20], [21]. In the AwAS-II design the stiffness can be varied between virtually no stiffness and infinitely stiff (rigid). This is done by varying the pivot point along a lever arm that is used to actuate a compliant spring element, Figure 1. Jafari et al. initially designed this device for use in safe man-machine interfaces, but the idea could easily be modified to into a torsion adaptor.

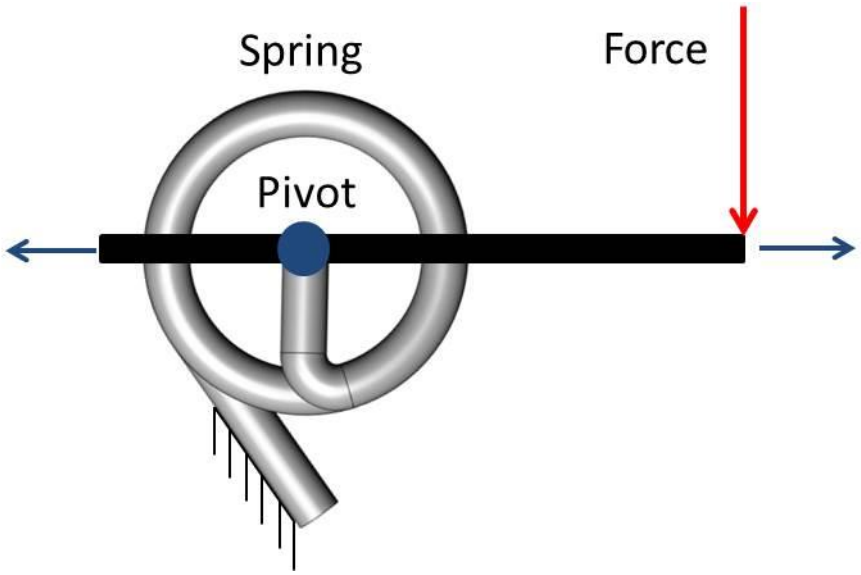

Figure 1: Adjustable Pivot Conception Layout

The size and mass of the device are ranked as a four. This moderately high rating is due to the fact that the device can utilize a smaller electric motor similar to the AwAS-II's Kollmorgen QT-0707 weighing only 1.6 oz, with an overall design weight of 1.1 kg [20]. Functionally this device only receives a three. While it has nearly infinite range for stiffness magnitudes, it has only one stiffness profile determined by its physical geometry. Its ability to change stiffness while under load or while rotating is untested. Power consumption is rated as a five. Electrical energy is only being consumed when the device changes stiffness levels, and is purely mechanical during normal operation at a single stiffness setting. Also, the direction of action to change the pivot point is perpendicular to the spring deflection motion and so the motor does not have to work against the springs in order to change stiffness levels when the device is

unloaded [20]. The failure condition of this device it receives a four. If the motor were to fail it would merely be stuck at its last stiffness setting and could still function manually if needed. Lastly, the cost of this unit was evaluated as a four. This is due to the smaller, less power intensive motor, allowing for a smaller battery, and lower costs. The composite score for this device is a 23.5.

2.1.2 Planetary Gear

The next possible design uses a gear setup. This system by Kim et al. [22] was also originally intended for use in safe interactions between machines and humans. The planetary gear system by Kim et al. consists of both position actuation (PA) as well as stiffness modulation (SM) which is each controlled by an independent motor. Modulation of the neutral position is a beneficial feature but was not a design consideration for this project, and is not covered in the scope of this thesis. Consequently, the PA will not be detailed here.

Stiffness modulation is achieved via a back-drivable SM motor while the PA motor is fixed. Kim et al. modulate the current to the SM motor in turn modulating the resisting torque of the electric motor which consequently adjusts the stiffness between the two links relative to each other. The relationship between the motor current and stiffness are fixed based on the design of the gears between the two links [22].

The design as it relates to the VSTA (stiffness modulation only) requires very few components, a motor and a gear set. However, depending on the torque requirements of the system, it could require a large motor to handle the torque requirements of the lower limb, or a large gear set to make the torque reduction. Kim et al. show data for the device producing up to 4 Nm of torque, only a third of the 12 Nm maximum torque produced by the intact human limb [18]. Kim et al. do not state any size or weight specifications as their work was to simply demonstrate their concept rather than actual function. While this design may prove to package in a relatively small space for use as the VSTA, it will most likely have a considerable weight.

Because of these factors and the unknowns surrounding this design it was given a score of three for size and mass. The function of the device was scored as a four. As a stiffness modulator, it would have infinite ability to change stiffness instantaneously under load and no load conditions. However, as the two links are attached directly through the drive train, there would be no damping in the system and stiffness modulation could seem coarse as the electric motor is modulated, depending on the control scheme. In regards to power consumption, this design was given a two. This is because stiffness modulation and torque holding require the electric motor to have current flow at all times. This means that even while standing still the device will consume battery power. There are only two main components that can fail, the motor or the gear train. In the event of a motor failure this design would effectively lose all stiffness, and would possibly significantly reduce the mobility of the user. A gear train failure would have a similar effect, earning a rating of two. Lastly, the potential cost of this design was given a rating of three. While there are relatively few components, the motor and gear set could potentially have a high cost. The motor would require a high torque capacity, and must have an accurate encoder to ensure accurate function. The power requirements denote a large battery pack, also increasing cost. The overall score for this design was 17.5.

2.1.3 Series Elastic Actuator

Series elastic actuators (SEA) have been used in robotics, rehabilitation, as well as designed for variable stiffness prosthetics [23]–[25]. A standard SEA layout consists of an electric motor, gearbox, and elastic element in series, Figure 2.

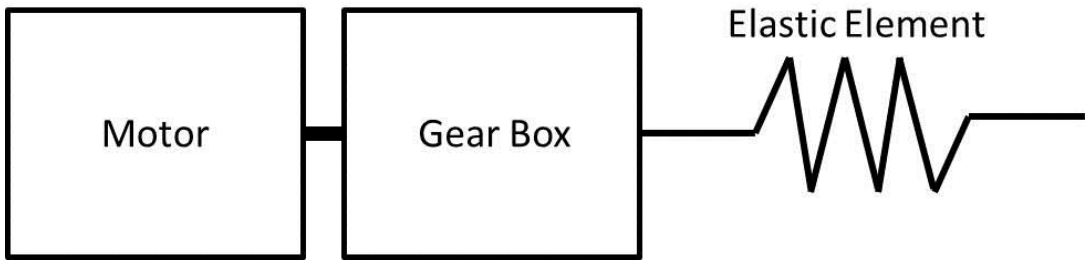

Figure 2: General Layout of an SEA

Similar to the planetary gear concept discussed previously, the electric motor is used to modulate the stiffness of the system with the gearbox used as a torque reduction to the system. The compliant element added to the end can also act as an inexpensive torque sensor by knowledge of the compliant elements stiffness and displacement. The elastic element also provides shock protection between the device and the user [24]. The eSEAJ prototyped by Lagoda et al. will be used as a baseline for the ranking system [24].

The eSEAJ presented by Lagoda et al. is 3.175 kg, 185 mm tall and 109mm in diameter [24]. This makes it considerably larger than the prototype presented for the variable pivot design, but within the 3.97 kg limit for additional prosthetic weight [26]. Because of the large mass, this design received a three for size and mass. Functionally this device received a score of five. This is due to its infinite capability to modulate torque, and ease of controllability given the input from the elastic element, and basic position sensors. Power consumption of this type of device would be high as the motor must be running at all times in order to modulate and hold torque, resulting in a score of two. Failure condition was scored a two as a failure of any of the three components would result in a complete failure of the device to hold torque. Cost was scored as a three as there are very few components, however, an electric motor with the capacity to drive the torques necessary would be expensive, and given the estimated power consumption the battery would likely be large. All combined, the SEA scored a 19.5.

2.1.4 Variable Length Elastomer

The last possible concept considered to vary torsional stiffness is presented by Schuy et al. [27]. This device uses a cylindrical elastic element that is twisted to produce torsional resistance. An actuator is used to adjust the effective length of the elastomer cylinder, and the stiffness of the device can be modulated [27]. This actuator can be made relatively small because it only acts to change the effective length and does not work directly against the torque in the device.

Schuy et al. presents a maximum length of the elastomer at 100 mm, however, this value could be greatly reduced depending on the elastomer used. Because of its modular ability which could make it relatively small, and its need for an actuator that does not work directly against torsion in the device, the size and mass was rated as a four. Functionally, the minimum and maximum stiffness of this device is limited by the material and geometry of the elastic element. Another limitation is that it is untested for modulating stiffness under load. Because of these limitations, it received a score of two functionally. Power consumption of this device would be low. The actuator is only drawing power when changing the stiffness, and is inert when at a static stiffness setting. Also, because the actuator does not work against the torque, it would take little to no effort to modulate the stiffness and receives a score of five. The failure condition of this device received a score of four. Similar to the variable pivot design, a failure of the actuator would still leave the device functional at a single stiffness setting that could be modulated manually. Cost was scored as a four. Because of the low power consumption, smaller actuator requirement, and simple elastomer design, this device would be relatively inexpensive. Overall this concept scored a 21.5.

2.1.5 Design Concept Ranking

Based on the evaluations performed for each design concept (see Table 1), it was decided to pursue the VSTA as a variable pivot adapted for transverse plane motion. Design of the VSTA is detailed next section.

Table 1: Scoring of Possible Device Designs

Criteria	Criteria Weighting	Variable Pivot	Planetary Gear	SEA	Elastomer
Size and Mass	1	4	3	3	4
Functionality	2	3	4	5	2
Power Consumption	1.5	5	2	2	5
Failure Condition	1	4	2	2	4
Cost	0.5	4	3	3	4
Total Score with Weighting		**23.5**	**17.5**	**19.5**	**21.5**

2.2 Design Criteria

Criteria were established in order to guide the design and modeling of the device. These criteria were split into two groups: structural and functional. An initial dimensional goal was set based on the 76 mm diameter of a standard prosthetic adaptor plate similar to those seen in Figure 3. This represents an ideal diameter that will integrate seamlessly into existing hardware.

Figure 3: Attachment Plates for Lower Limb Prosthetics

The device is intended to be installed in the pylon of an existing prosthesis, Figure 4. The length of a pylon is variable, depending on variables such as residual limb length, patient height, and the particular hardware the patient is utilizing (foot and, if applicable, knee). Because of this, the height must be kept to a minimum in order to fit into existing pylon space.

Static load structural requirements, Table 2, were the next design criteria considered and are the main consideration for the casing. Structural requirements were derived mostly from the ISO 10328:2006 *Prosthetics--Structural testing of lower-limb prostheses—Requirements and test methods*, as well as a theoretical bending load. The bending load is set by a crouching scenario (Figure 5) with anthropometry values set by a 50th percentile male with the maximum load set by the ISO 10328:2006 standard. This scenario involved in a 254 mm lever arm with 65 kg of load at the end resulting in a 163 Nm bending load on the outer housings. It is most optimal to have the device as close to the knee as possible as this will decrease the moment of inertia for the limb during swing, and have less influence on the swing dynamics of the limb while walking. These structural standards represent near worst case static scenarios and will most likely not be encountered by the initial proof of concept prototype, but give a good starting point for design and analysis.

Figure 4: Device Placement

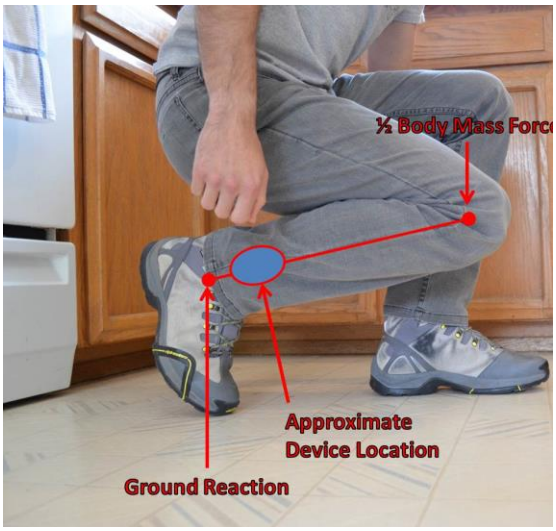

Figure 5: Maximum Bending Condition

The functional requirements (Table 3) of the design have to do with its ability to perform the tasks necessary to be a successful variable stiffness torsion adaptor. These were derived primarily from background research of existing torsion adaptors on the market, prototype devices, and the capabilities of the intact human ankle. The main criteria for these were stiffness capabilities, range of motion, and device mass and size. Capabilities of an able bodied walker provide a basis for the design requirements. It has been shown that the human ankle is capable of a maximum torque of 11-12 Nm around 15-20° of internal rotation, and a maximum rotation of 26° [18], [28]. Maximum device mass was set to 3.97 kg, as it has been indicated that this mass can be added to a lower limb prosthesis with no significant effect on self-selected walking speed of the amputee [26]. Using the information gathered, the VSTA's 1:1 spring rate was targeted at 0.6 Nm/° and a range of +/- 30°.

Table 2: Structural Requirements for a Lower Limb Prosthetic Device

Load Condition	Max Load	Reference
Compression	130 Kg	ISO 10328, A100, Condition I
Torsion	65 Nm	ISO 10328, A100, Condition I
Bending	163 Nm	Calculation in Text

Table 3: Functional requirements for a torsion adaptor

Torsion Range	Spring Rate	Device Mass	Device Size	Device Basis	Reference
+/- 20°	0.23 Nm/°	No Data	No Data	Existing Device	[8]
±30°	0.5, 0.6, 0.7 Nm/°	379 g	No Data	Existing Device	[18]
360°	Variable	3.175 kg	No Data	SEA Prototype	[24]
+/- 17°	Variable	1.1 kg	0.18mx0.14m	AwAS-II Prototype	[29]
360°	Variable	No Data	45x61x41mm	Planetary Gear Prototype	[30]
+/- 20°	0.8 Nm/°	Not Applicable	Not Applicable	Intact Ankle	[16, 26]

2.3 VSTA Design

The design process consisted of three steps. Using the previously defined parameters, a SolidWorks (SolidWorks 2013; Dassault Systems; Waltham, MA) model was developed that met all the predetermined functional requirements. Next, a mathematical model was developed to characterize the physical motions and forces experienced by the VSTA and established criteria for motor selection. The solid model was then run through SolidWorks Motion and FEA analysis to visualize the operation of the VSTA and refine the design around the defined structural requirements. Lastly, a physical prototype was built and final design revisions were made based on limitations encountered during the manufacturing and assembly of the VSTA.

2.3.1 Solid Model Design

The proposed VSTA can be seen in Figure 6. Design of the VSTA was separated into three main subassemblies: Outer Housings (6-A/B), Slider (6-D), and Spring Carrier (6-E). All hardware in the VSTA was sourced using McMaster-Carr and are readily available off the shelf

with exception of the main spring. Initial design specifications of the VSTA model are shown in Table 4.

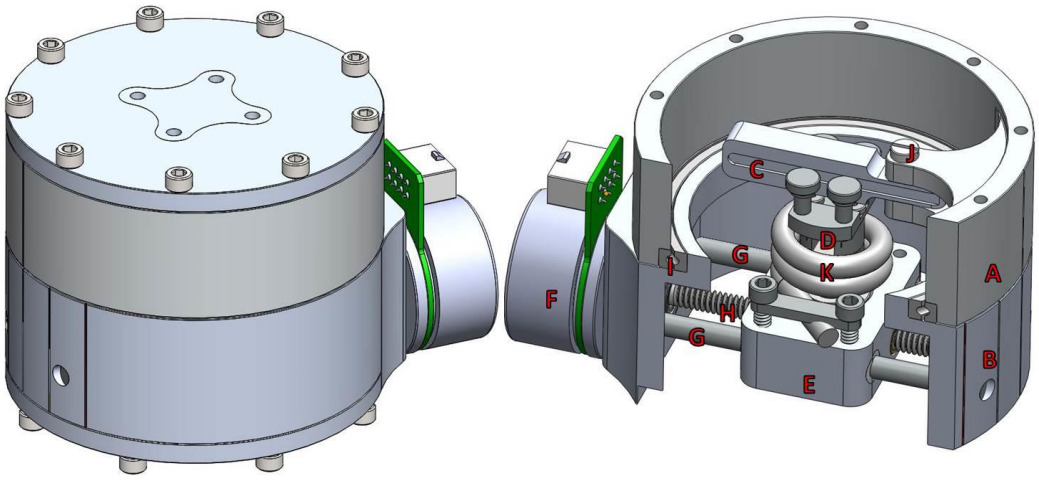

Figure 6: Variable Stiffness Torsion Adaptor. A) Upper Housing, B) Lower Housing, C) Lever Arm, D) Slider, E) Spring Carrier, F) Electric Motor, G) Guide Rail (2x), H) ACME Lead Screw, I) Main Bearing, J) Pivot Pin, K) Torsion Spring.

Table 4: Initial VSTA Design Specifications

Motion Range	Stiffness Range	Mass	Size
±30°	0.10-∞ Nm/°	1.27 Kg	89 mm tall x 111 mm Dia

The basic concept of the VSTA can be described as an upper and lower housing (Figure 6-A and 6-B respectively) attached via a main bearing (6-I), and can rotate relative to each other to provide the transverse plane movement. Attached to the upper housing is a lever arm (6-C) that is attached via a pivot pin (6-J). When the upper housing is rotated the lever arm forces the Slider (6-D) to rotate with it, displacing the torsion spring (6-K), which is grounded to the Spring Carrier (6-E) via a bearing. The Slider can be moved along the length of the lever arm via an ACME lead screw (6-H) rotated by and electric motor (6-F), moving the Spring Carrier along two guide rails (6-G). The Upper and Lower Housings, along with the Lever Arm are machined from 6061-T6 aluminum. Adjusting the position of the Slider along the Lever Arm changes the mechanical advantage of the Upper Housing over the spring, and so multiple stiffness values

can be achieved. The VSTA is symmetric for either direction of travel, and provides for a locked condition when the axis of rotation of the Slider and that of the Lever Arm pivot are aligned, Figure 7. However, the VSTA is limited such that it can only reach the lock position when the relative displacement of the two housings is at or near zero. The whole device is closed on either end by plates and filled with grease to ensure that all the components are well-lubricated to reduce friction, noise, and wear. The plates are drilled with the standard 4-hole pattern of the adaptor plate in Figure 3, which is also the same pattern as an adjustable pyramid, a standard prosthetic attachment device.

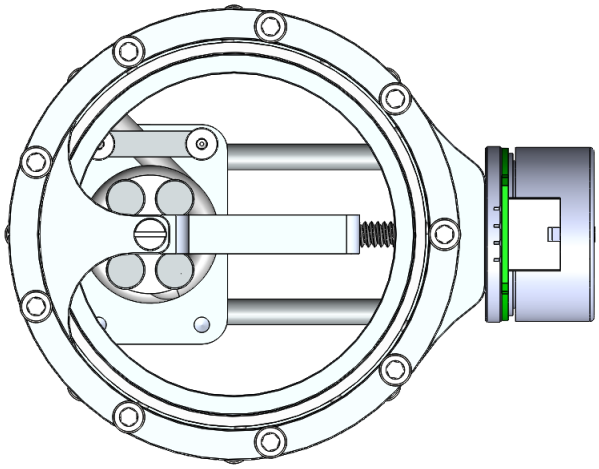

Figure 7: VSTA in "Locked" Position

The design goal of the housing diameter was initially driven by the 76 mm goal of the design criteria, however, clearance of the spring and main bearing became an issue (Figure 8-A) and so the outside diameter was increased to 4 3/8 inches. Other clearance issues had to be addressed such as the clearance between the Carrier and the Lower Housing (8-D), Carrier bolt heads and the Lower Housing (8-B), and the Slider components with the arm of the Upper Housing (8-C). These interference conditions are of most issue when the VSTA is in the Locked position.

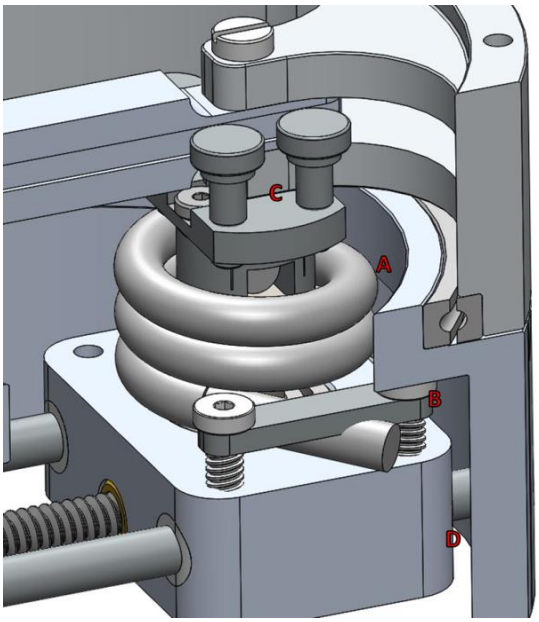

Figure 8: VSTA Clearance Concerns. A) Spring to Housing Clearance, B) Carrier Bolt Head Clearance, C) Slider Component Clearance, D) Spring Carrier to Housing Clearance

Actual minimum and maximum stiffness values necessary for the device are not known, and so the length of the Lever Arm was set arbitrarily at 38.1 mm (1.5”) in order to give the widest range possible in the package space. The length of the Lever Arm dictates how much travel was required for the Spring Carrier to reach the minimum stiffness and lock positions and so the main bearing and housings were sized accordingly as discussed above.

The rate for the ideal torsion spring was set at 0.6 Nm/° to match the mid-range adjustment of the existing device described by Flick et al. [31]. When the Slider is set to the center of travel along the lever arm, the VSTA has a 1:1 mechanical advantage over the spring. This means the mid-range value of the VSTA is also 0.6 Nm/° and can be adjusted in either direction from there. A commercial torsion spring of this rate was not found so one was designed specifically for this application using design equations found in [32]. The design requirements initially assumed for the spring are a rate of 0.6 Nm/°, 90° of deflection, and to fit within the confines of the VSTA. Because the VSTA could be designed around the spring to some degree, the actual dimensions are variable, but some minimum and maximum values were used to estimate the spring. Assumptions were a supporting rod diameter of 15.9 mm,

mean coil diameter of 25.4 mm (D), a minimum of three active coils (N), and a maximum deflection of 90° (F), and Music Wire with an Elastic Modulus (E) of 196500 MPa. At 90° of deflection the spring would be at 54 Nm of torque (T). The wire diameter was determined from:

$$d = \sqrt[4]{\frac{4000TND}{EF}} = \sqrt[4]{\frac{4000*54\ Nm*3\ coils*0.0254\ m}{196500e6*90°}} = 0.0055\ meters = 5.5\ mm \quad (1)$$

Also the minimum diameter of the spring when under load should be considered to verify that the support rod is not too large:

$$Loaded\ ID = \frac{ND_{free}}{N+\frac{F}{360}} = \frac{3\ coils*0.00254\ m}{3\ coils+\frac{90}{360}} = 0.023\ m = 23.4\ mm \quad (2)$$

These calculations show that the support rod is feasible, and might possibly be larger, or the mean diameter of the spring could be decreased if necessary giving more clearance for the bearing (Figure 8-A). Generally, the calculations indicate that a spring could be made to meet the requirements of the VSTA. However, after consulting spring manufacturers it was found that a maximum wire diameter (d_w) of 5.26 mm (0.00524 m in equations (3) and (4)), 3.8 active spring coils (N), and a mean coil diameter (D_m) of 31.8 mm (0.0318 m in equations (3) and (4)) the highest spring rate that could be manufactured to fit was 0.33 Nm/°. This number was determined by rearranging equation (1):

$$Spring\ Rate\ (\frac{Nm}{°}) = \frac{d_w^4*E}{4000*N*D_m} \quad (3)$$

Music wire has a maximum yield stress of 1758 MPa. A calculation of the stress in the wire:

$$\sigma = \frac{d_w*E*\theta}{392*N*D_m} \quad (4)$$

While the spring manufacturer indicated that this spring would be capable of deflections up to 90°, equation (4) indicates that the max stress in the spring will be reached at a deflection (θ) of 71°. This means that for the VSTA to maintain a full range of +/- 30° the carrier cannot be moved infinitely between the minimum stiffness and infinitely stiff. To avoid permanent deformation of the spring, the VSTA should be limited to maximum operating stiffness of 2 Nm/°.

The maximum stiffness is later updated to 1.17 Nm/° due to increased spring stress during counter-clockwise rotation. This result will be discussed later during the bench testing sections, and 1.17 Nm/° will be taken as the maximum from this point on. The infinitely stiff, locked position does not depend on deformation of the spring and so can still be used, but should only be activated when the VSTA is not under load. Five springs were ordered from two separate companies and tested before installation in the VSTA, which is discussed later.

The Slider sub-assembly (Figure 9) consists of the four track rollers (9-C), along with the Upper (9-A) and Lower (9-B) Support Rods. The Upper and Lower sections are held together by two 10-24 low head bolts. The Upper Support Rod has a window (9-D) that is slightly undersized in depth to the spring wire diameter. The two halves of the support rod clamp around the top spring arm securing it to the support rod such that the spring deflects with the Slider when rotated. The lower end of the Lower Rod tapers down to meet the shaft diameter of a bearing in the Spring Carrier, supporting the Slider while allowing it to rotate. Design of the dimensions and materials of the Slider are discussed later in the FEA section.

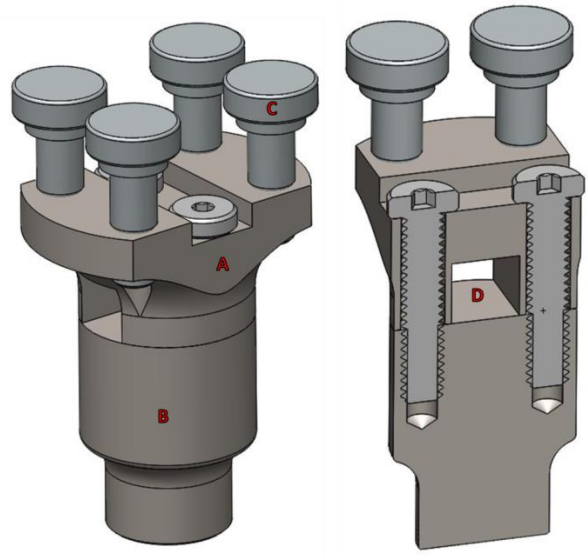

Figure 9: Slider Sub Assembly. A) Upper Support Rod, B) Lower Support Rod, C) Track Roller (4x), D) Spring Clamp Window

The Spring Carrier (Figure 10) consists of the main Block (10-A) machined from 6061-T6 aluminum, Slider support bearing (10-B), Spring ground clamp (10-C), Guide Rail Bushing

inserts (10-D), threaded bushings (10-E), and the spring (10-F). The spring is grounded to the main block with the clamp. This allows for the spring to deflect when the Slider is rotated by the Lever Arm. The guide rail inserts are four linear bearings to support the Carrier block, while allowing it slide freely along the guide rails (Figure 6-G) when the stiffness of the VSTA is being adjusted. The brass threaded bushings are the interface between the ACME lead screw (Figure 6-H) and the Carrier and provide for lower friction on the threads than a direct-threaded aluminum interface with the Carrier Block.

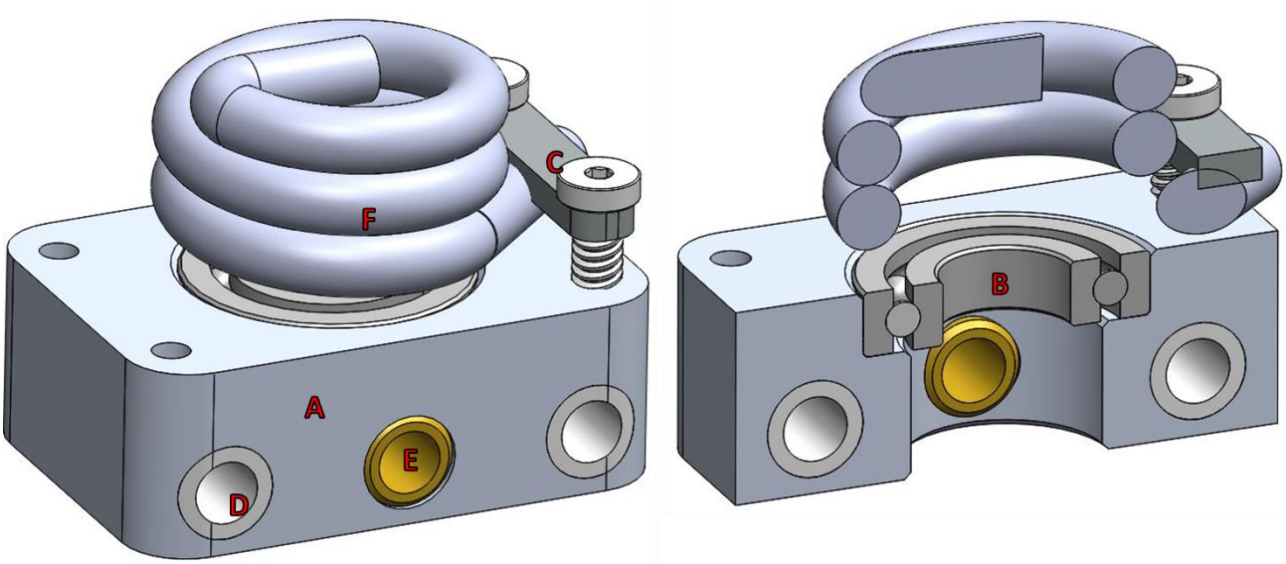

Figure 10: Spring Carrier Sub Assembly. A) Main Block, B) Slider Support Bearing, C) Spring Ground Clamp, D) Guide Rail Bushing, E) Lead Thread Bushing, F) Spring

An ACME lead screw was chosen due to its availability and acceptable friction properties when compared to a standard bolt thread while still being resistant to back driving when the Carrier is under load. This means that the motor only needs to be under power when adjusting the stiffness, and does not need to use battery power to maintain position. Initially, a ball screw was considered for this position due to its extremely low friction, but would most likely result in back driving of the Carrier under high loads, and so was not a viable option.

2.3.2 Mathematical Model and Motor Selection

The model is based on the geometric interactions of components in the VSTA with the stiffness depending primarily on the length of the lever arm. Because the rotational axes of the spring and the VSTA housings are not necessarily aligned, as the housing rotates the actual lever arm length changes. The lever arm length is measured from the lever arm pivot to the spring center. With the VSTA at zero deflection, the spring offset is equal to the lever arm length. As the VSTA rotates, the lever arm length will change as the lever arm pivot is moved relative to the spring center. This change in lever arm length is more drastic the farther the spring offset is from the VSTA center (Figure 11).

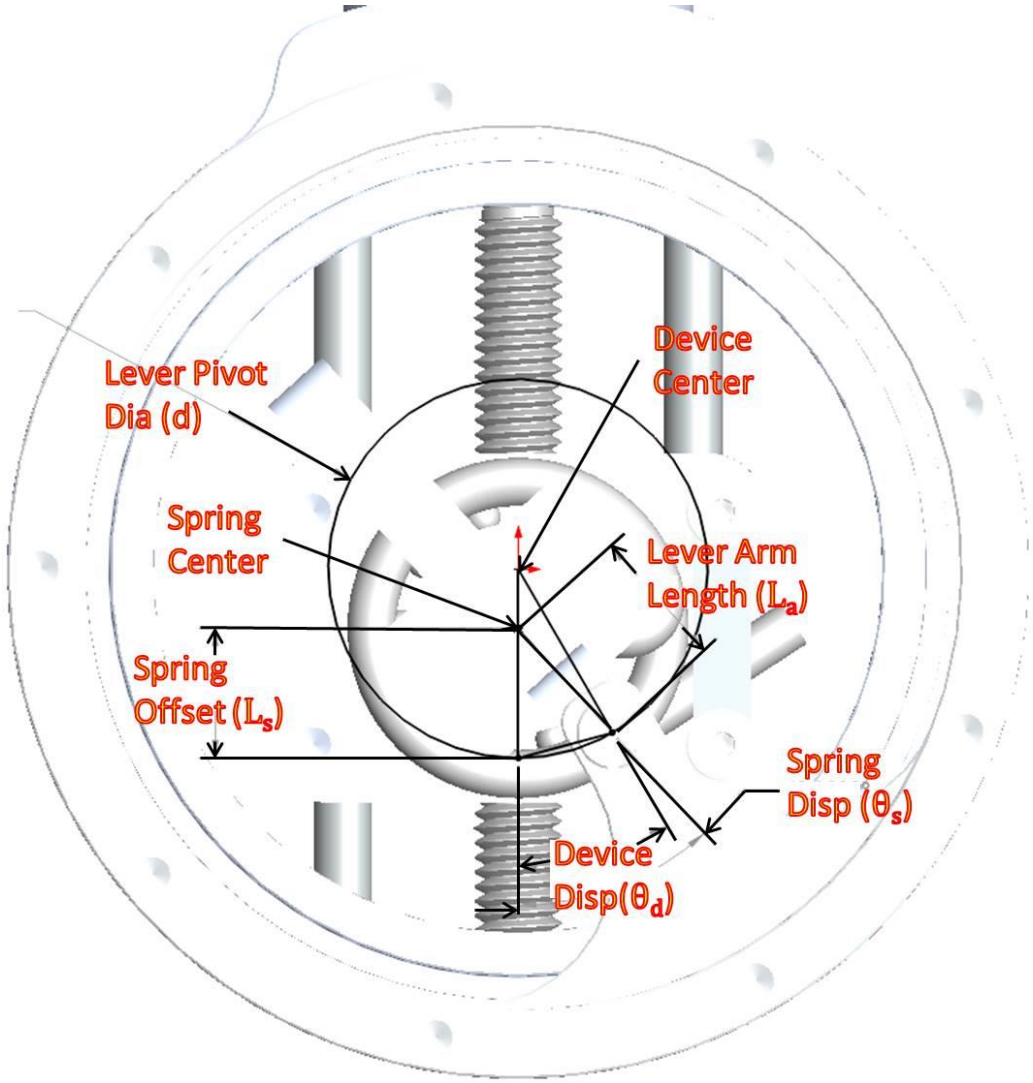

Figure 11: Geometric layout of VSTA. This top view shows how the geometric relations between the lever arm and the spring center offset change as the VSTA is deflected. In the depicted orientation, the spring offset is closer to the lever pivot than the device center. As the lever pivot sweeps along its diameter, the lever arm will effectively lengthen.

Using the length and angular relations between the components, the length of the lever arm (L_a) can be found based on the distance the spring center is offset from the locked position (L_s), the rotational displacement of the housings (θ_d), and the diameter of the lever pivot pin circle (d) in the upper housing:

$$L_a = \sqrt{\left(d sin\left(\frac{\theta_d}{2}\right)\right)^2 + {L_s}^2 - 2d sin\left(\frac{\theta_d}{2}\right) L_s cos\left(\frac{180-\theta_d}{2}\right)} \quad (5)$$

Using the length of the lever arm and the displacement of the VSTA, the displacement of the torsion spring (θ_s) can then be determined:

$$\theta_s = sin^{-1}\left(dsin\left(\frac{\theta_d}{2}\right)\frac{\sin\left(\frac{180-\theta_d}{2}\right)}{L_a}\right) \quad (6)$$

Knowing the displacement of the spring and the 0.33 Nm/° designed spring rate, the torque in the spring (τ_s) can be calculated and related to the resulting VSTA torque (τ_d):

$$\tau_d = \frac{d\tau_s}{2L_a\cos(\theta_s-\theta_d)} \quad (7)$$

Modeling of the device torque, τ_d, for any fixed carrier position, L_s, through the displacement range of the VSTA (+/- 30°), was achieved utilizing equations 5-7. Figure 12 shows predicted torque curves for the VSTA for several discrete settings of the lever arm position. It can be seen that the VSTA has a relatively linear torque response through the range of motion. As the stiffness of the VSTA is increased the torque curve gradually becomes less linear as a result of the lengthening of the lever arm during operation.

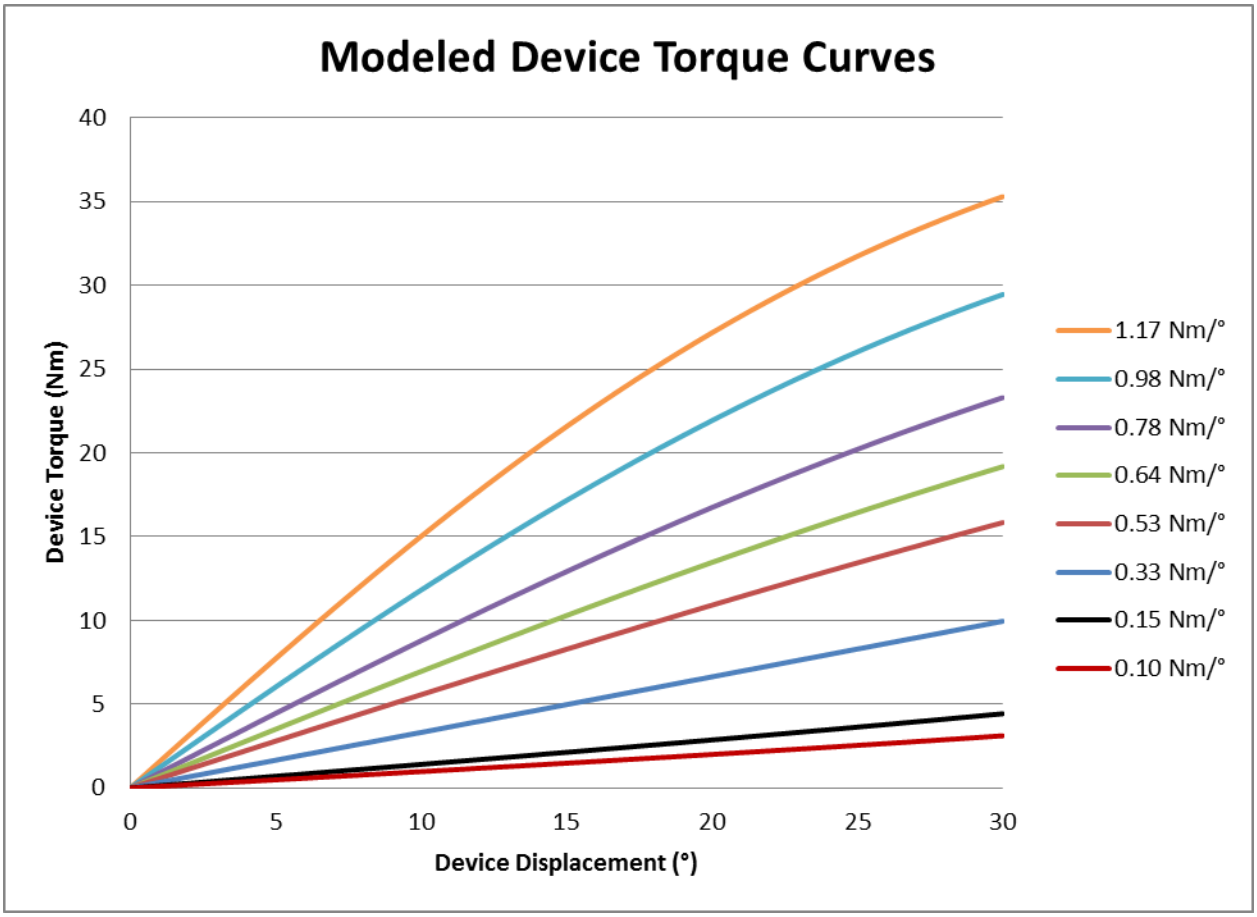

Figure 12: Modeled torque curves for the VSTA at eight different static settings between the maximum and minimum stiffnesses.

An electric motor is used to position the spring carrier and determine the stiffness of the VSTA. Ideally, the motor should have the capability to change stiffness even at peak deflection, and so a calculation was performed to determine the necessary torque requirements. The force needed to push the carrier to the maximum torque condition (1.17 Nm/°) was calculated as the component of the forces parallel to the rails that guide the carrier:

$$F_c = \frac{\tau_d}{d}\sin(\theta_d) \tag{8}$$

The peak electric motor torque can be determined by the previously calculated linear force on the carrier. This is derived from the spring displacement (θ_d), the mean thread diameter (d_m), the lead of the acme screw (L), and the coefficient of friction (*f*) between the steel screw and the brass bushing taken as 0.16 for greased steel on brass [33]:

$$\tau_m = \frac{F_c d_m}{2} \frac{f\pi d_m - L}{\pi d_m - fL} \quad (9)$$

The resulting peak motor torque was calculated at 180 Nmm. Using this information, a Maxon EC 45 Flat Motor (PN 397172, Maxon Motor AG, Switzerland) was selected as it had a nominal torque capacity of 130 Nmm and a stall torque of 820 Nmm.

Motor speed for stiffness changes was also evaluated. Stiffness changes during initial testing will be done between trials or in the swing phase of gait when torsional load is zero. Swing phase times are variable between 0.19-0.25 seconds for adults [34]. Without knowing the mechanical properties of the system it is difficult to estimate the actual time it will take for the motor to accelerate and decelerate, and what peak speed the motor will reach. As a best case estimate the motor speed of 6110 rpm will allow for variation from the minimum to maximum stiffness in 0.24s. While this time is at the high end of the range of the specification, it will be sufficient for initial testing.

2.3.3 Motion and FEA Analysis

Characterization of the VSTA at individual stiffness levels through the entire range of motion (±30°) was completed to better visualize the operation of the VSTA, Figure 13. Initial motion analysis was completed on the premise that the VSTA torsion spring would not be stress limited, and as such includes analysis of positions beyond the capability of the final VSTA.

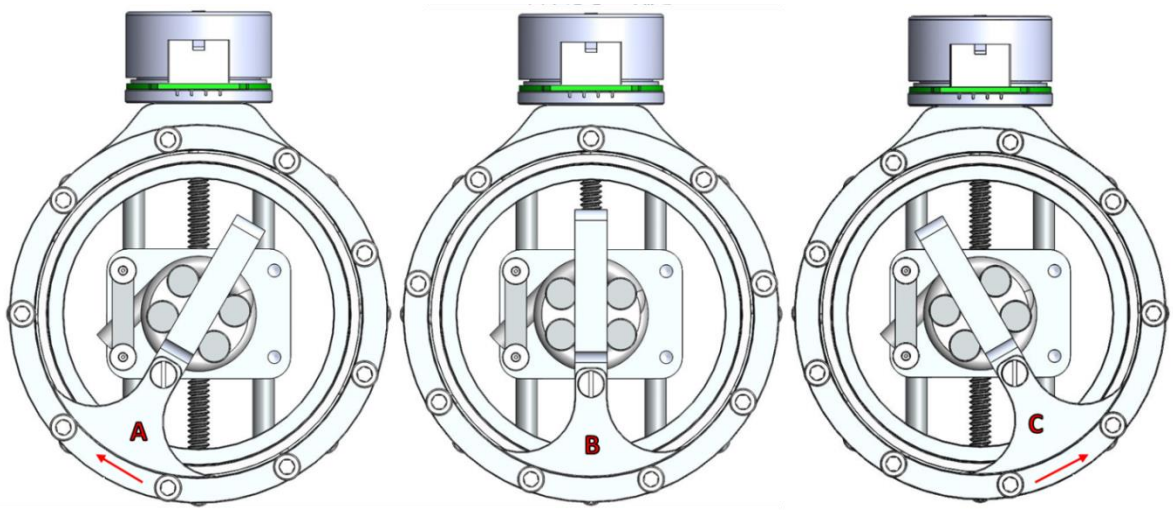

Figure 13: Angular displacement of housing with slider held at VSTA center, VSTA displacement equal to spring displacement. A) -30° Position, B) 0° Position, C) 30° Position

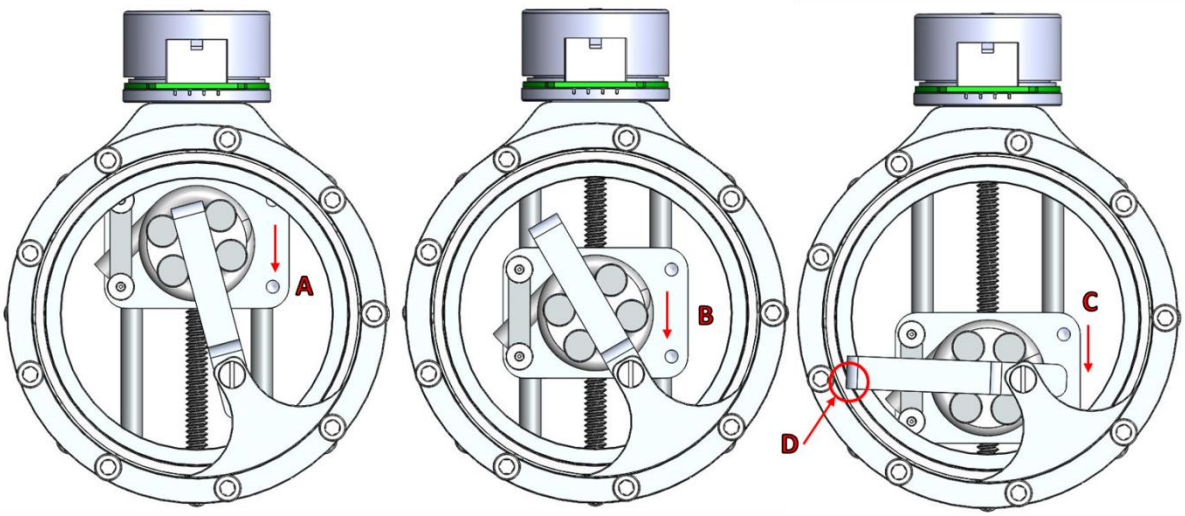

Figure 14: Movement of VSTA when housing displacement at 30° maximum. A) Minimum stiffness setting (0.1 Nm/°), B) Median stiffness setting (0.33 Nm/°), C) Maximum stiffness setting, geometrically (3.55 Nm/°), D) Lever arm contact with housing at maximum position

Geometrically the highest stiffness level available set by travel interference between the Lever Arm and the inside of the Upper Housing (Figure 14-D) would be approximately 3.55 Nm/° if the spring were robust enough to allow it.

The FEA analyses tested many of the static load conditions experienced by the VSTA. While a factor of safety (FOS) of at least two was a goal, and would be necessary at a minimum for a mature product, the design of the prototype aimed for a minimum FOS of one. This was

deemed sufficient because this prototype is mostly a proof of concept and research device to better understand the benefits of variable torsion, and so will most likely not ever be exposed to the highest load conditions. The structural requirements derived from the device criteria section led to compression, and bending analyses, Figure 15 and Figure 16, respectively. The bending scenario detailed in Figure 5 was modeled as depicted in Figure 17 with the lower section of the individual housing grounded and one half the body weight applied at the end of the arm. Both upper and lower housings passed the compression FEA with a FOS of 2.23, and 1.98 respectively. Both housings also passed for bending, with a FOS of 1.14, and 1.12 respectively. The torsion moment from the ISO standard was of greatest concern for the maximum force exerted on the Lever Arm mount of the Upper Housing while the Device is locked, Figure 18. This is simulated by applying the maximum torsion of 65 Nm to the upper housing while the pivot pin hole is held by a bearing fixture. Initially, the thickness of the arms was undersized and this analysis helped identify the appropriate thickness to withstand the maximum moment condition while in the locked position.

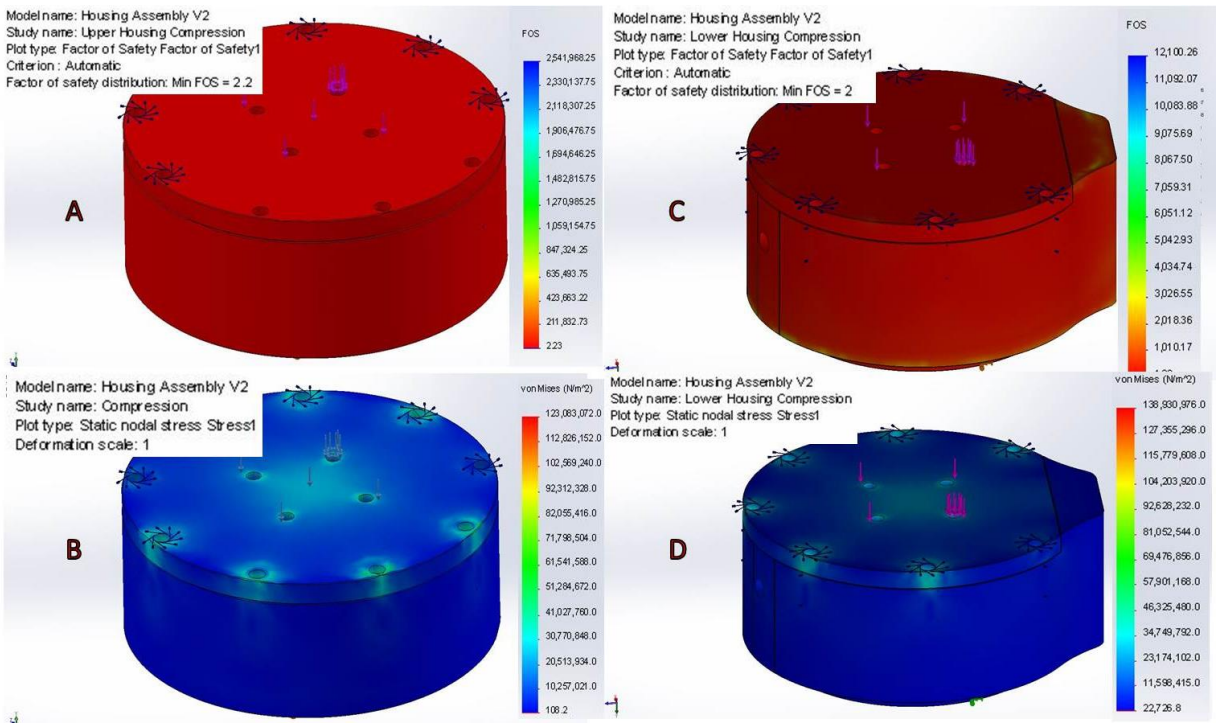

Figure 15: Upper and Lower Housing Compression FEA. A) Upper Housing Compression FOS Plot (Min 2.23), B) Upper Housing Compression Stress Plot, C) Lower Housing Compression FOS Plot (Min 1.98), D) Lower Housing Compression Stress Plot

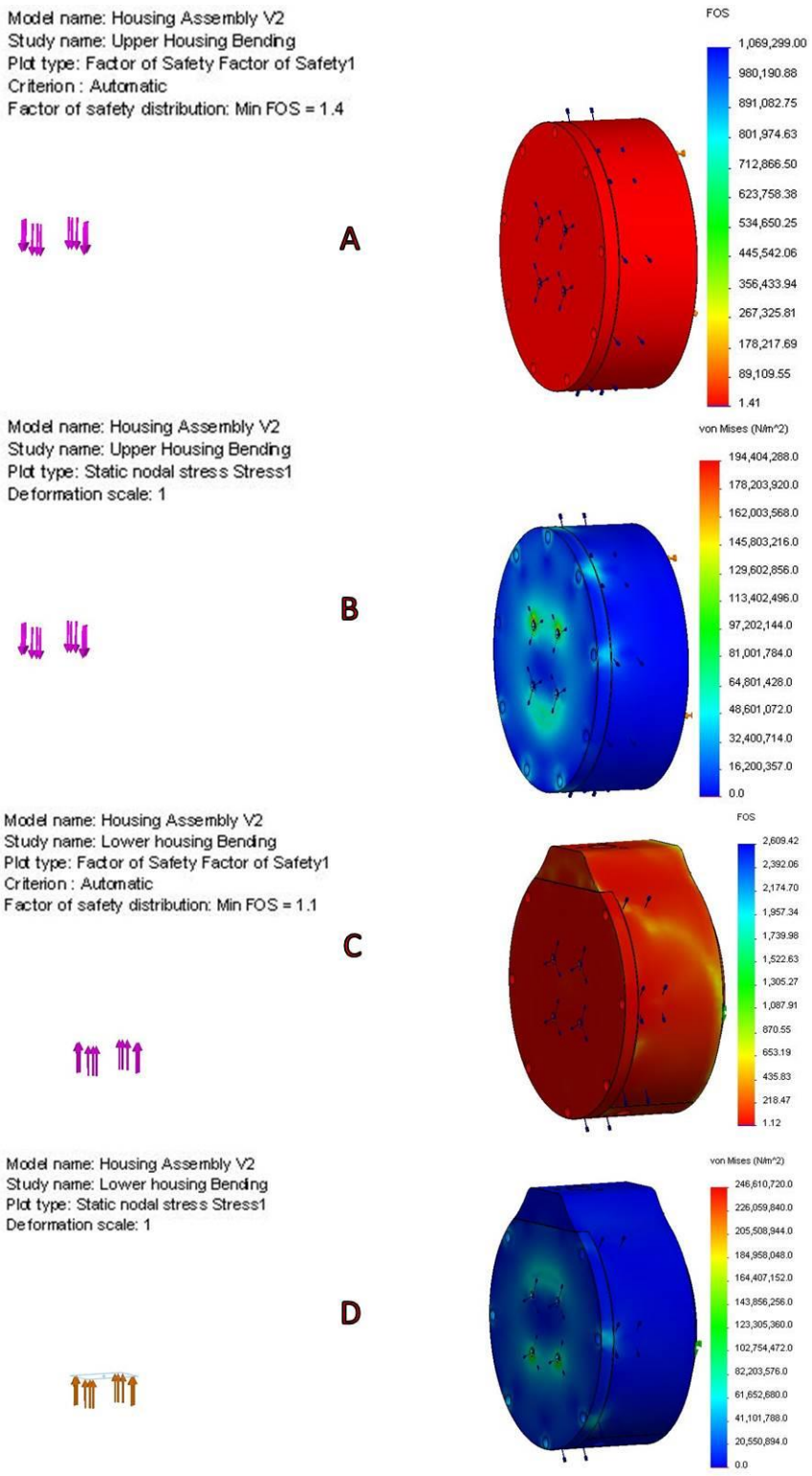

Figure 16: Upper and Lower Housing Bending FEA. A) Upper Housing Bending FOS Plot (Min 1.41), B) Upper Housing Bending Stress Plot, C) Lower Housing Bending FOS Plot (Min 1.12), D) Lower Housing Bending Stress Plot

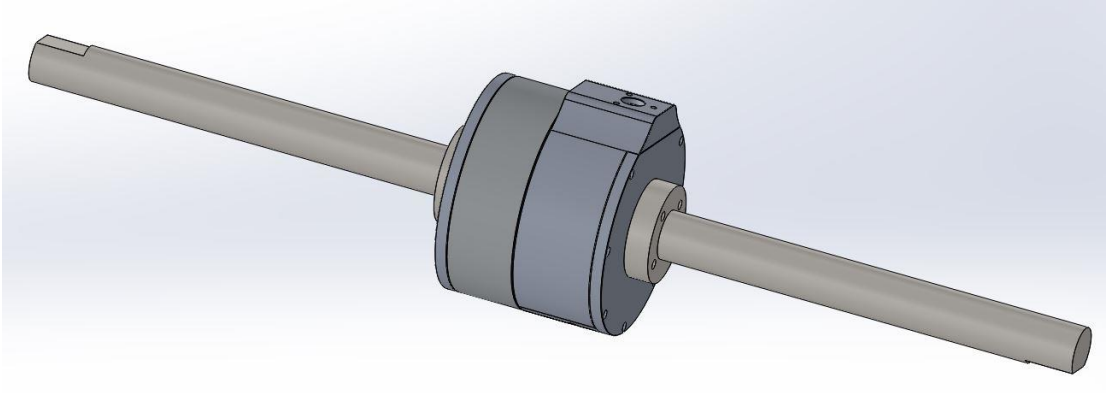

Figure 17: Housing Bending CAD Setup, Load applied at end of rod to simulate bending scenario detailed in Figure 16

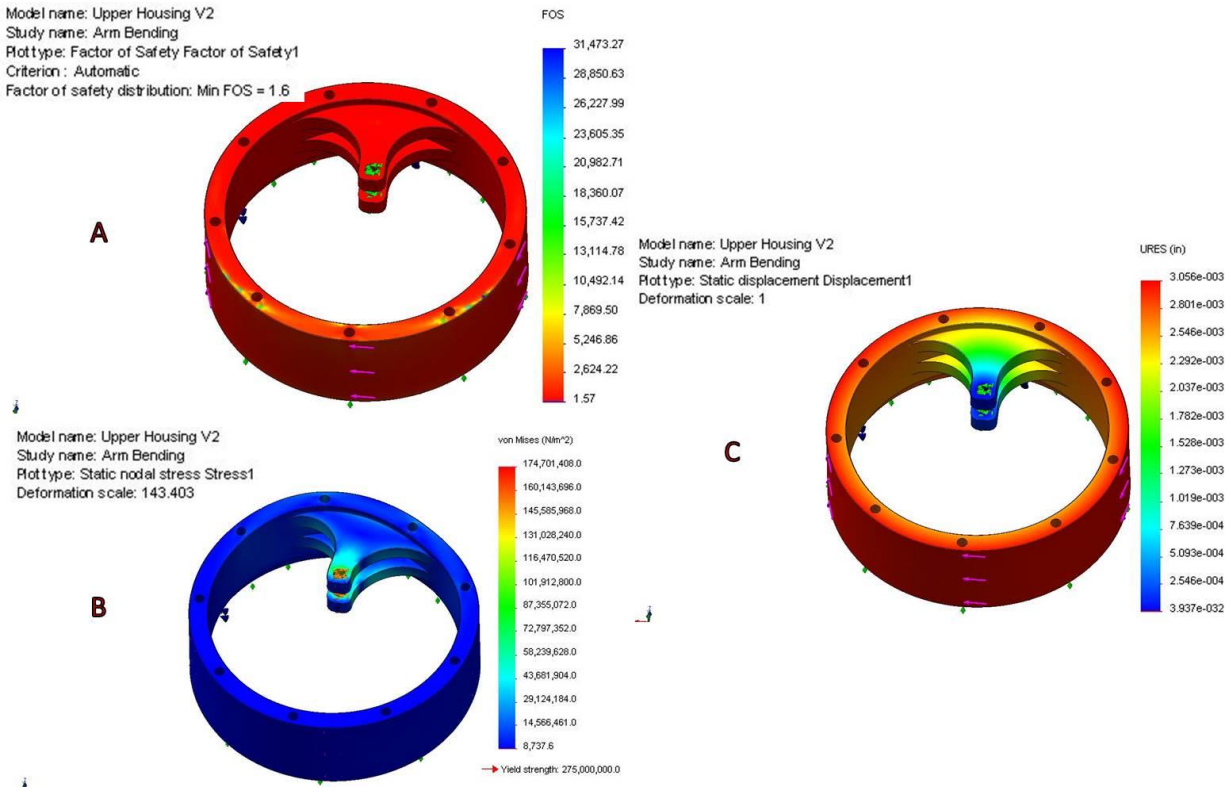

Figure 18: Lever Arm Mount FEA , Max Torsion While Locked. A) FOS Plot (Min 1.57), B) Stress Plot, C) Deflection Plot (Max 0.0762 mm)

The linear load determined in the mathematical model also gave a basis to test the Slider. This was modeled as a bending load at the track rollers with the slider grounded in the bearing of the Carrier, Figure 19. This lead to increases in diameter of the Upper and Lower Slider along with a material change from 6061-T6 aluminum to 4340 heat treated steel in order

to meet maximum load requirements. Even after performing these changes, the design only reached a FOS of 0.9, 0.1 short of the design goal. A redesign was avoided as it would require a larger bearing in the Carrier which would exceed the local size limits and cause a major redesign of multiple components. It was deemed appropriate as-is since this load condition modeled will most likely not be encountered in operation, and can be controlled and monitored carefully in testing to verify the design.

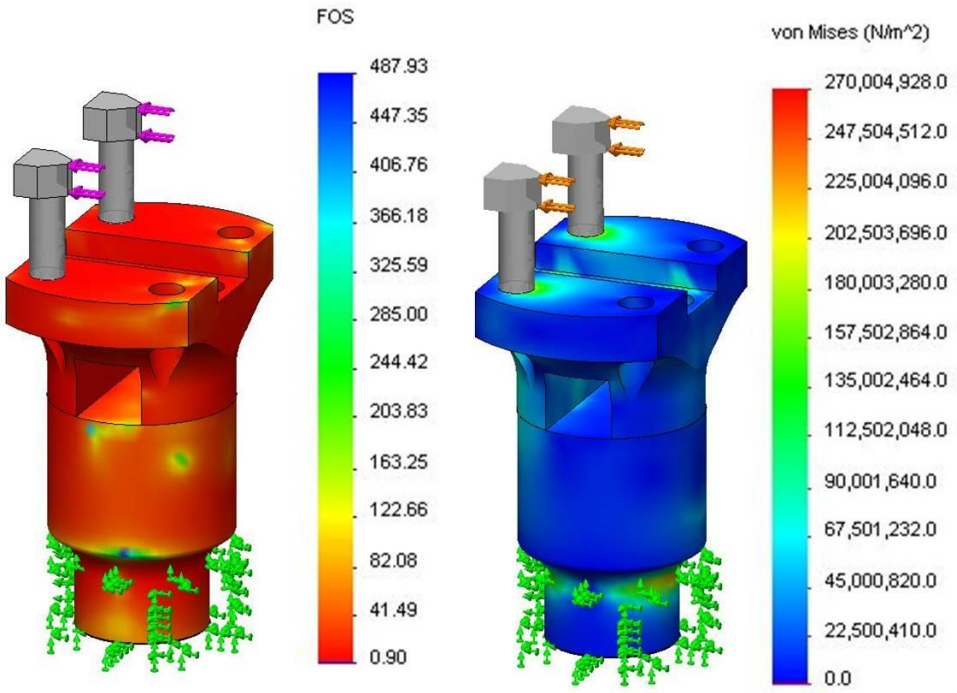

Figure 19: Slider Bending FEA. A) FOS Plot (Min 0.9), B) Stress Plot

The initial prototype design of the VSTA followed an iterative approach that focused on function, and ease of manufacturing. In the interest of manufacturing, more exotic materials such as titanium alloys and carbon fiber were not considered for this design as they can be difficult to work with, and in the case of carbon fiber difficult to model with respect to the actual result when making custom parts by hand. To further ease design for this project, only static loads were evaluated. As the design matures, and testing is completed to better refine the functional requirements of the device, a more in depth analysis should be completed. This will

include evaluation of the cyclic loading of the device over its intended life span as this is the mode of failure for a device of this type. As it stands, this prototype design has an increased size and weight from the initial design goals, but provided a solid base for laboratory research testing that will allow further refinements of the design criteria.

2.3.4 Design Change in Manufacturing

While every attempt was made to manufacture the prototype exactly as the design dictated, issues were encountered once the design was brought to prototype. The primary design deviation occurred with the interface between the track rollers and the lever arm. It was found that the track rollers initially specified were incapable of supporting the loads exerted on them. While a new design with larger capacity rollers was developed, the budget and timeframe of the project did not allow for the new components to be purchased. As such the interface was modified to use already purchased material.

The interface between the slider and the lever arm was modified to have the slider head contact directly along the lever arm, Figure 20-A. While this design will most likely cause the mechanism to bind under load, disallowing for stiffness changes under load, it was decided that for initial testing the VSTA would only be operated at discrete stiffness settings, and not varied while under load, which will be discussed later.

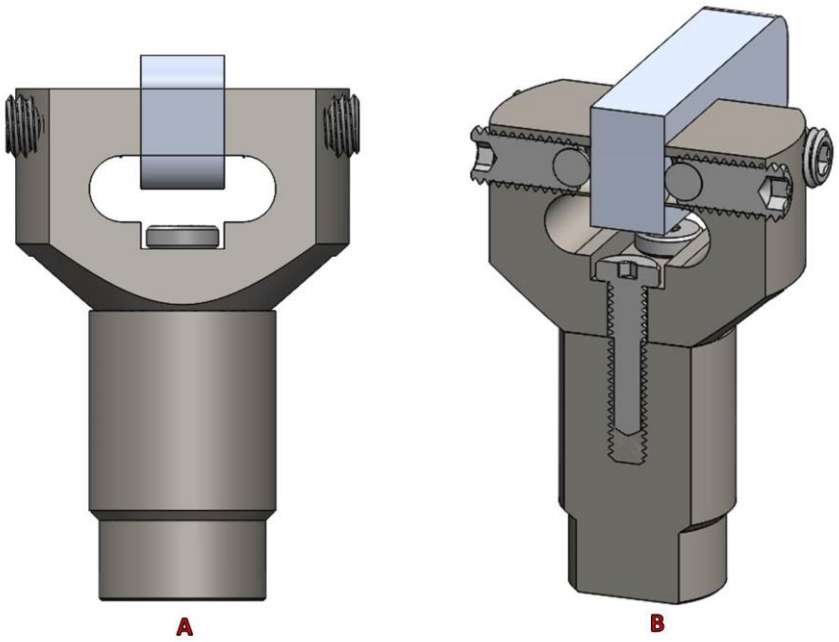

Figure 20: Modifications to Slider A) Single piece slides along lever arm replacing track rollers, B) Four ball head set screws interface directly with lever arm to allow for tolerance adjustment.

Due to manufacturing tolerances there was a small gap between the width of the slider head and the thickness of the lever arm. To remedy this, four ball end set screws were added to allow for the adjustment of contact between the slider and the lever arm, Figure 20-B. To accommodate the new interface, the material of the lever arm was changed from 6061-T6 aluminum to 4340 hardened steel. This was to help prevent damage to the lever arm from high stresses concentrated at the head of the ball set screws when the VSTA is under load.

3 Mechanical Bench Testing

Mechanical bench testing was performed first on the custom torsion spring to determine the actual rate of the manufactured product, and second on the VSTA as a whole to compare its actual behavior with the modeled results. Bench testing was performed using a servo-hydraulic material testing system (Model 858 Bionix™; MTS System Corporation, Eden Prairie, MN). Both the spring and the VSTA were tested with three repeated trials at 0.5°/s, and three repeated trials at 60°/s in both the clockwise and counter clockwise directions through their full motion

ranges. These values were based on testing by Flick et al. used to evaluate torsion adaptor products currently on the market, and are used as a basis for comparison [18].

3.1 Spring Testing

Springs were tested in the MTS to determine their actual spring rate for comparison to the calculated values. These tests compared the physical springs to their design specifications. This allowed for a spring to be selected for use in the VSTA.

3.1.1 Spring Testing Methods

Two springs from each manufacturer were tested for comparison with a fifth spring tested for use in the VSTA. Two manufacturers were used to make springs for testing: Sound Spring (Kent, WA) and Diamond Wire Spring Company (Tyler, TX), SS and DW, respectively. Springs were attached in the MTS to simulate how they will be mounted in the VSTA in an effort to get an accurate portrayal of spring performance, Figure 21.

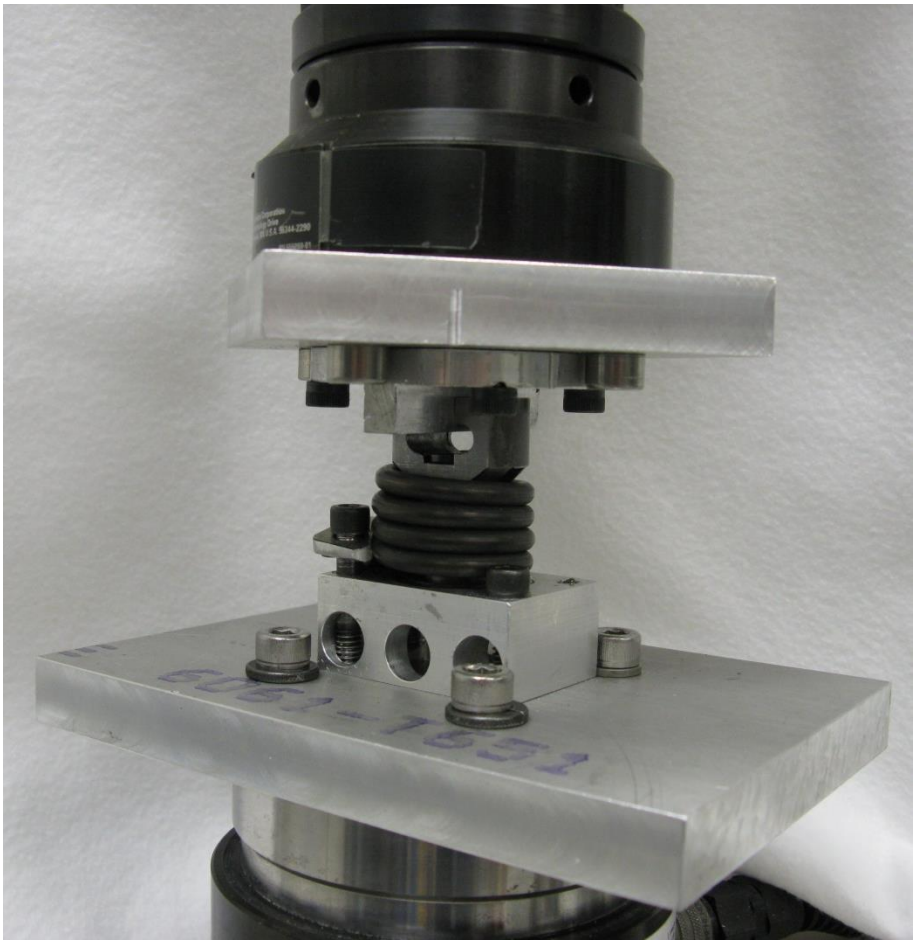

Figure 21: Spring testing fixture on the MTS

Springs were initially tested to 90° of deflection, as this was prior to spring stress analysis, and had been indicated as acceptable by the manufacturer, but as discussed before this exceeds the stress of the spring design and causes permanent deformation to the spring. Springs manufactured by SS were deemed unsatisfactory of use in the VSTA during testing. When deflected in the counter clockwise direction the upper tang experienced total failure. Because of this, only results in the clockwise (CW) direction can be reported for SS springs. It was also found through trial and error that deflecting the spring in the counter-clockwise (CCW) direction (against the wind direction) resulted in higher spring stresses and permanent spring set [32]. A deflection of 57° was determined iteratively from the testing results and used for the counter-clockwise direction to alleviate this issue. Given these discoveries during initial testing,

the final spring used in the VSTA it was tested to the calculated 71° in the clockwise direction (direction of spring winding), and to 57° in the counter-clockwise direction.

3.1.2 Spring Test Results

Results showed that there was variation between each of the springs, and that a certain spring must be chosen carefully to achieve the desired result in the VSTA. Springs from SS manufacturer are shown first. Two springs from SS were initially tested, with only results in the CW direction shown due to failure in the CCW direction, Figure 22 and Figure 23. For this and all subsequent figures regarding MTS trials the key is read as: Specimen Number, Trial Number, Displacement Range, Manufacturer, Displacement Direction, Rate. For example, the label: “1.1, 0-90, SS, CW, 0.5” describes the first spring and first trial for that spring on the MTS, a deflection from 0-90°, manufactured by SS, and deflected in the clockwise direction, at a rate 0.5 °/s. The data from testing the SS springs in the clockwise direction showed that the springs had relatively linear loading paths, with little difference in load rate by initial inspection. Also, it was noted that the spring hysteresis was consistent between trials.

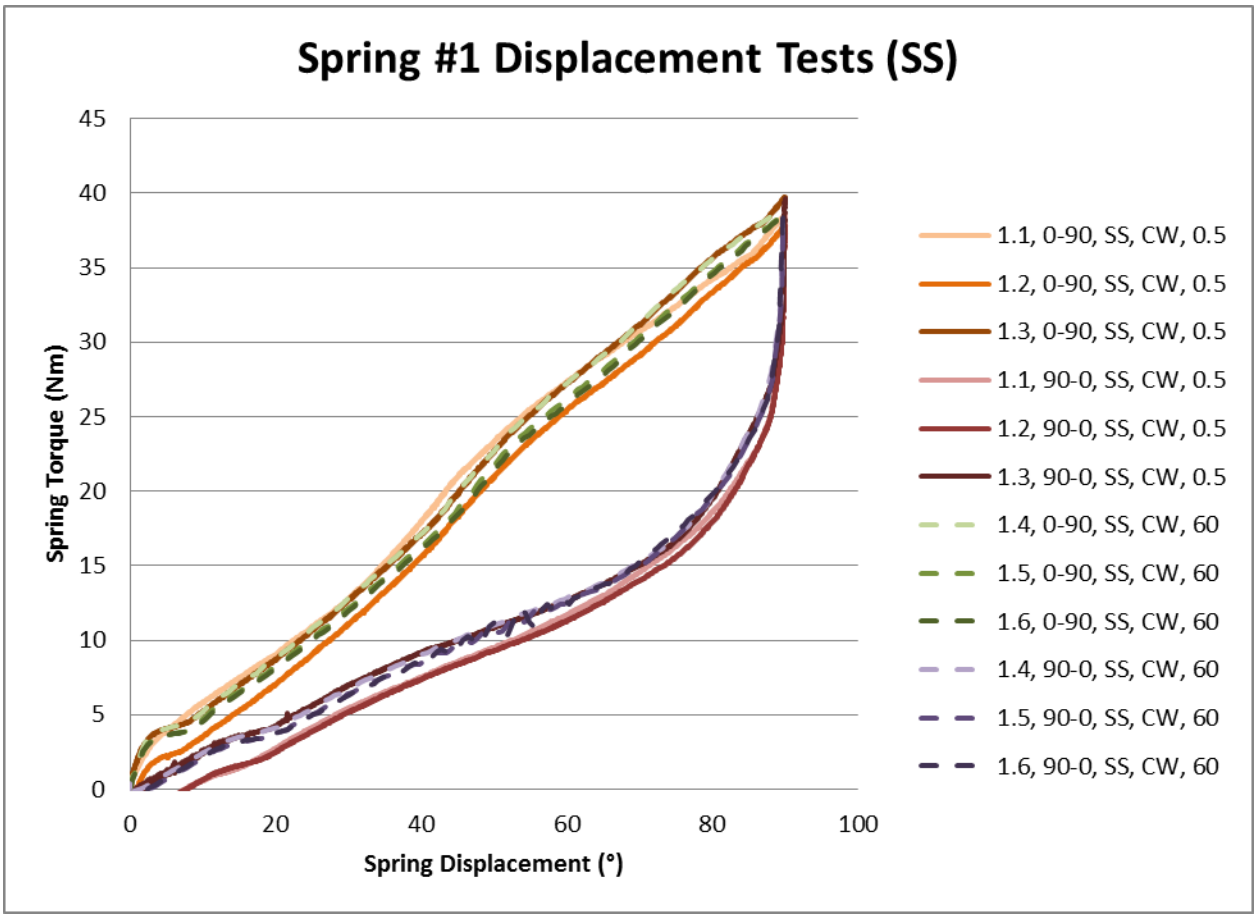

Figure 22: Spring 1, manufactured by SS. Trials in the CW direction only due to CCW failure. This spring showed a loading rate of approximately 0.4 Nm/°

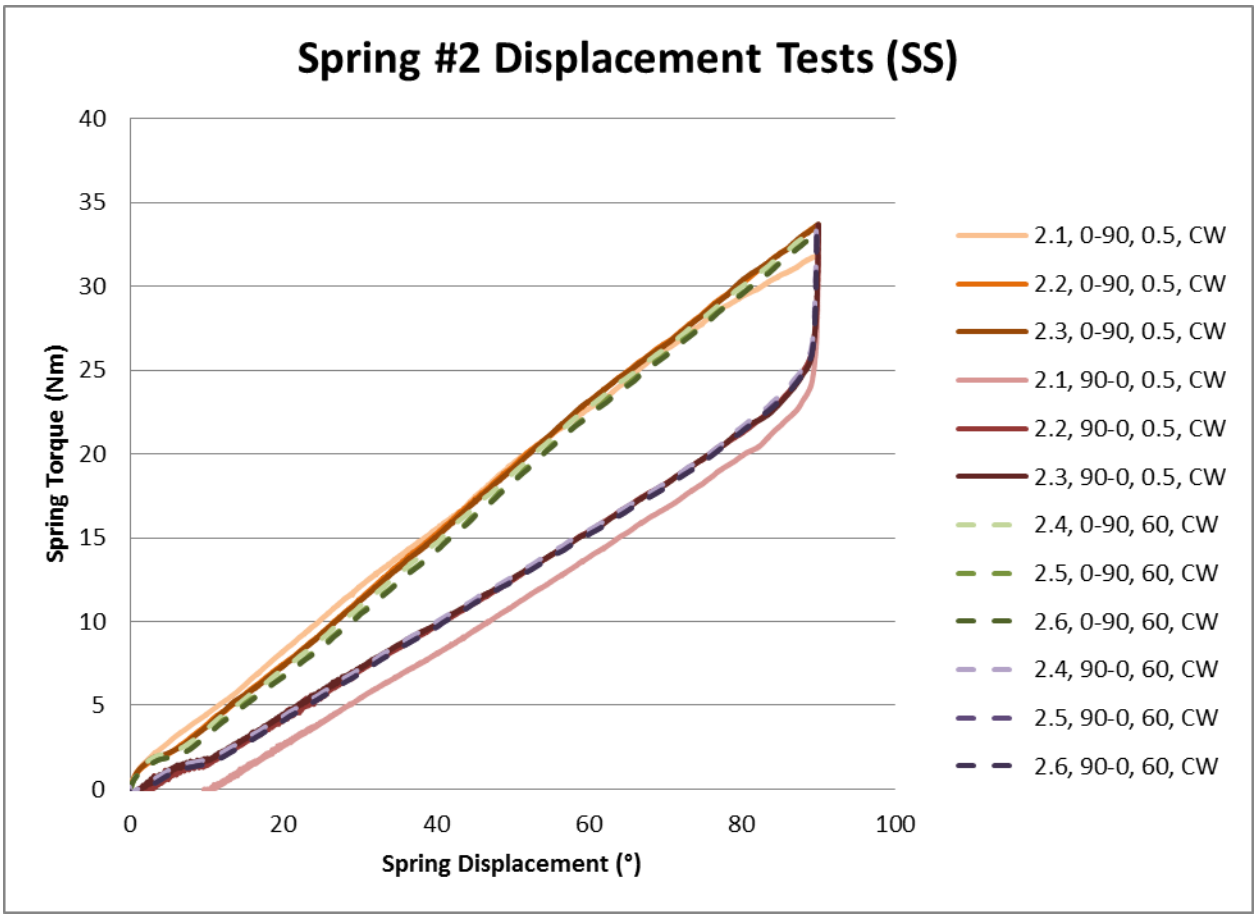

Figure 23: Spring 2, manufactured by SS. Trials in the CW direction only due to CCW failure. This spring showed a loading rate of approximately 0.36 Nm/°

Due to spring failure, all springs from SS were not considered for use in the VSTA. Testing continued with springs from the second manufacturer, DW. Similarly these springs were tested to displacements of 90° in both the CW and CCW directions. As a metric to characterize the spring's loading capacity, only the loading characteristics of the springs were necessary (0-90° data). Hysteresis data (90-0°) for DW springs was found to be similar to that of SS springs, and so unloading data is omitted from the graphs in an attempt to make them more readable. Data from DW springs can be found in Figure 24 and Figure 25. All charts showing data in the CCW direction display displacement and torque as absolute values. This was done to better compare the CW and CCW slopes against each other. Figure 24 shows testing on specimen three DW, and a significant difference can be seen between the CW and CCW trials with

significant variation between individual trials. This was a result of deflecting the spring to 90° in both directions, resulting in over stress of the spring that caused variation in the spring performance.

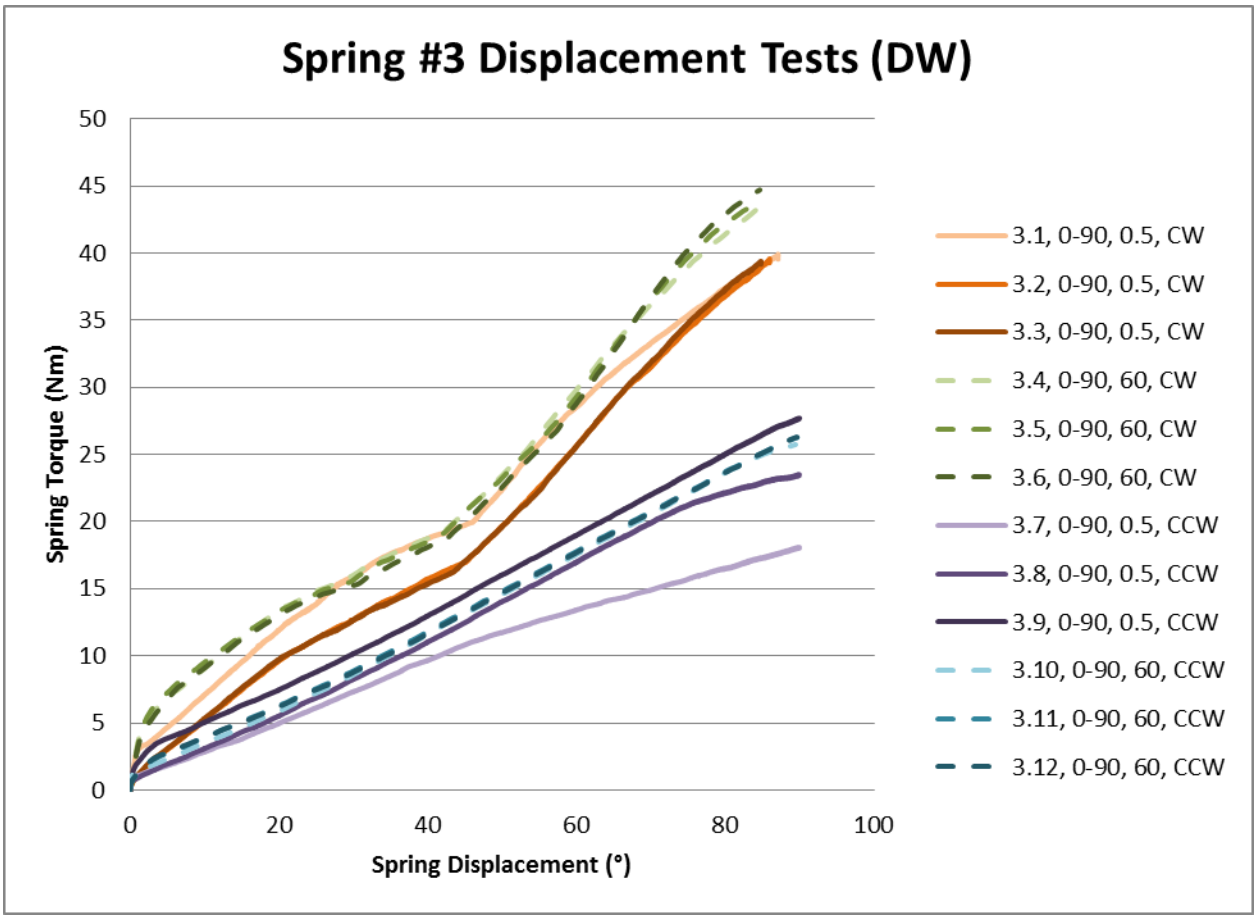

Figure 24: Spring 3, manufactured by DW. This spring showed a CW loading rate of 0.45 Nm/°, and a CCW loading rate of 0.27 Nm/°

In an attempt to limit spring stress variations, repeated trials to 90° in the CCW direction were limited for spring four. Figure 25, showing spring specimen four, has slightly less variability between trials than specimen three, but still indicates a significant difference between CW and CCW performance.

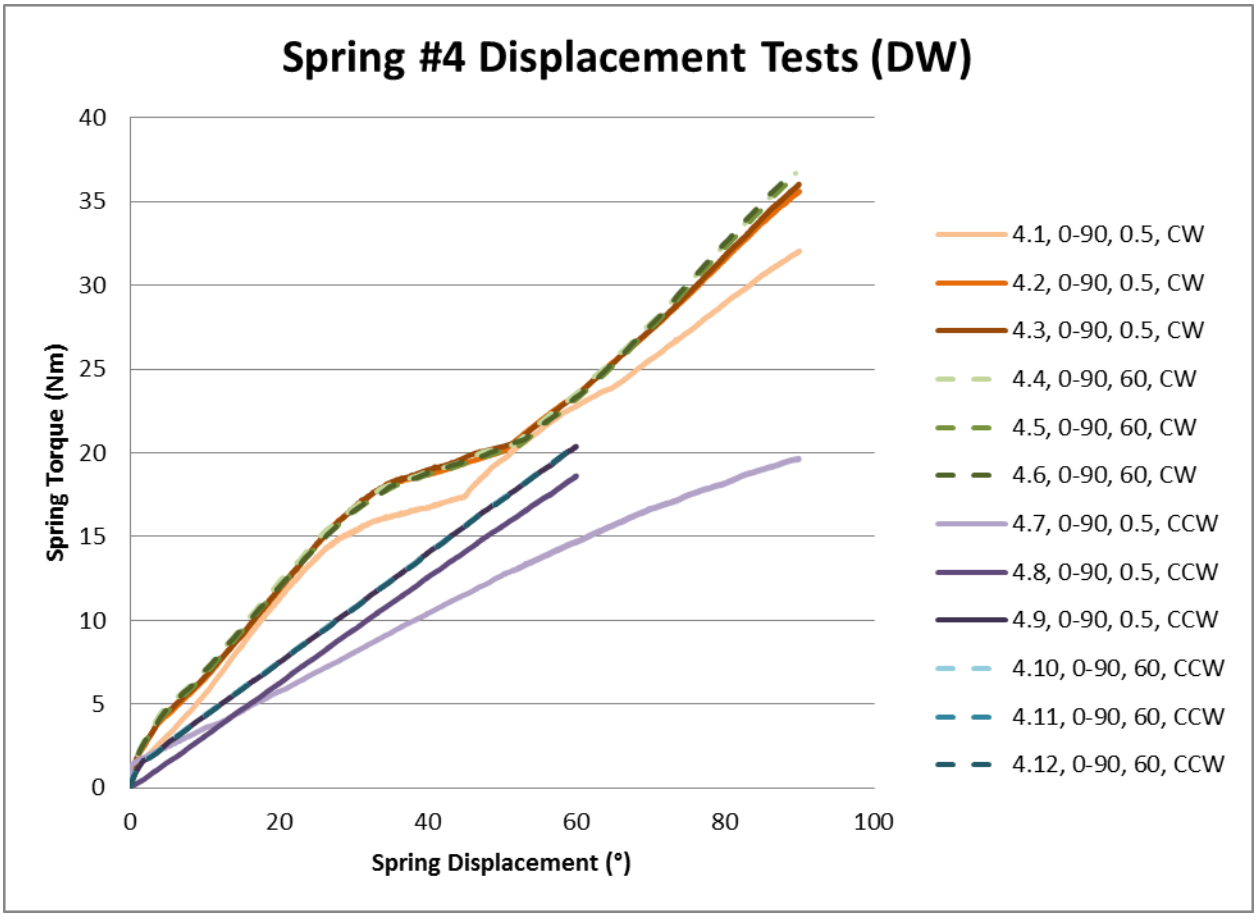

Figure 25: Spring 4, manufactured by DW. This spring showed a CW loading rate of 0.40 Nm/°, and a CCW loading rate of 0.27 Nm/°

Initial trials on the two DW springs confirmed what the spring calculation predicted, that deflection to 90° would cause excessive stress in the spring. The maximum spring deflection calculation presented earlier is only valid for the CW direction as traditional torsion springs are not rated for deflection in the direction opposite of the wind. The spring design guide [32] indicated that deflection in the direction opposite the winds would produce the same spring rate, but would result in higher stresses, and shorter spring life. As the VSTA is a prototype and not intended for long term use, this compromise was deemed acceptable for the design, however, no method for determining spring stress in the direction opposite the wind could be found. To determine the maximum displacement in the CCW direction testing of springs three and four were performed iteratively at increasing deflections until a maximum deflection was found. By

deflecting the spring to different angles and determining which deflections did not result in permanent spring set, a maximum deflection of 57° in the CCW direction was determined.

Using the information from the initial four spring tests and the calculations of spring stress, a fifth spring was tested to be used in the VSTA. This spring testing was limited to 71° in the CW direction and 57° in the CCW direction to prevent damage to the spring before being installed in the VSTA, Figure 26. Spring five testing can be seen to have much greater consistency between trials, with a similar spring rate between the CW and CCW directions. A comparison of the differences in spring rate between the varying conditions is shown in Table 5. The data in Table 5 is taken only for displacements from 0-57° and shows the comparison of the tested spring rates between the varying conditions of CW, CCW, 0.5 °/s, and 60°/s. Spring rates were determined as a best fit linear trend line forced through the origin for each dataset. It was decided that the VSTA would be limited in both directions by 57° of spring deflection to help prevent overstress of the spring, and also because the spring loading curves in the CW and CCW directions matched best up to that value. It can be concluded that the differences in spring rate between both spring deflection speed and spring deflection direction are insignificant at less than 1% difference between the test variables.

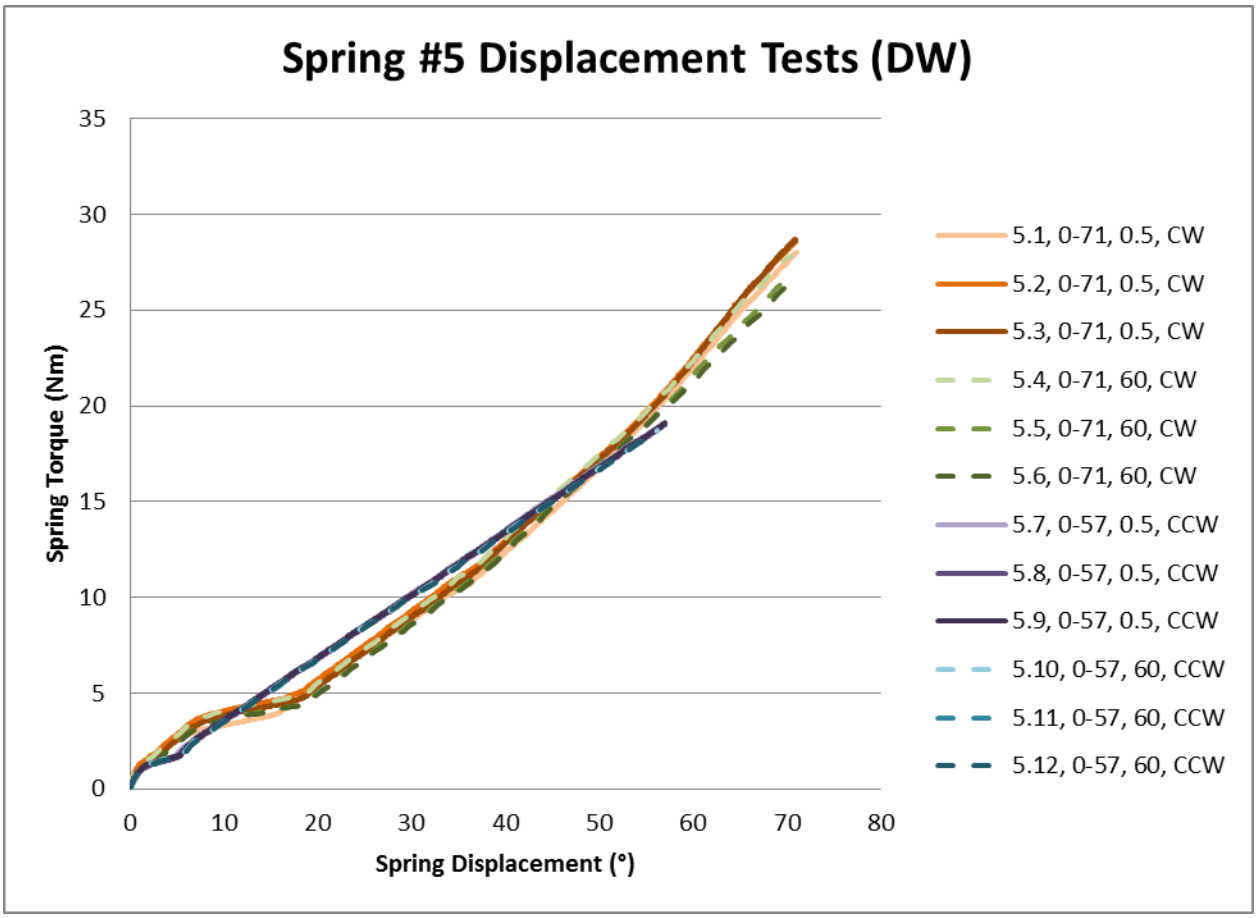

Figure 26: Spring 5, manufactured by DW. This spring showed a symmetric loading rate of 0.33 Nm/° for both CW and CCW directions.

Table 5: Comparison of Spring 5 Performance for displacement 0-57°

Comparison	CW: 0.5 vs 60	CW 0.5 vs CCW 0.5	CCW: 0.5 vs 60	CW 60 vs CCW 60
Percent Difference	0.18%	0.98%	0.27%	0.89%

Spring 5 exhibited far better characteristics than its predecessors and was deemed a good candidate for installation in the VSTA.

3.1.3 Spring Testing Analysis

After testing multiple springs, one was found that was suitable for the VSTA. Initial spring testing on specimens 1-4 yielded poor results. The first four springs were inconsistent between trials and exhibited different rates between CW and CCW loading, however, did show that loading rate did not have an effect on spring characteristics. It was also found that the springs manufactured by the SS manufacturer were incapable of being loaded in the CCW direction without failure of the spring tang. This could be due to a manufacturing error in materials, but was not investigated further since the DW spring was deemed acceptable. These variations in testing can be attributed to the over stressing of the springs by deflections up to 90°. As presented previously, the springs reach their maximum stress at 71° of CW deflection and approximately 57° of CCW deflection. When the fifth specimen was tested without exceeding the stress tolerances, it was found to perform as expected from the spring design. The spring loaded at a rate of 0.33 Nm/° as predicted in the spring design, with less than 1% difference in rate between the 0.5 °/s and 60°/s loading rates. Spring 5 did show some difference in loading pattern between the CW and CCW directions, particularly past 57° of deflection. To accommodate for this, and to help reduce the chance of failure, the VSTA will be limited in testing to not exceed 57° of deflection in the CW or CCW directions. This will effectively limit the highest unlocked stiffness to 1.17 Nm/°. While this is less than the original design, it is still greater than the numbers reported for current devices and has the capability to reach the torque levels of the intact human ankle [16, 26].

The spring performs as expected given its geometry. When the spring is loaded in the CW direction it is contracting the spring diameter and effectively adding active coils, while in the CCW direction the spring is expanding and subtracting coils. This behavior accounts for the different stresses in the spring and can account for the varying behavior of the spring when loaded in different directions. Traditionally, coil springs of this type are only meant to be loaded

in the direction they are coiled as opposite loading can significantly reduce spring life [32]. While this situation is not ideal for a mature market product, it is deemed acceptable for this prototype that will experience significantly lower forces and cycles than a product used on a daily basis. In the future, the design should be revised to accommodate long life and high stress in both the CW and CCW directions.

3.2 VSTA Testing

Following spring testing, the VSTA was assembled with spring five and tested to determine its actual operating parameters as compared to the models used during the design phase. Physical testing also allowed for the identification of design modifications necessary before moving on to human subjects testing. These modifications were discussed earlier in the design modifications section. VSTA testing results and analysis are then discussed.

3.2.1 VSTA Testing Methods

The VSTA was assembled with spring five and setup on the MTS as it would be connected in the pylon of a prosthesis, using pyramid adaptors, Figure 27.

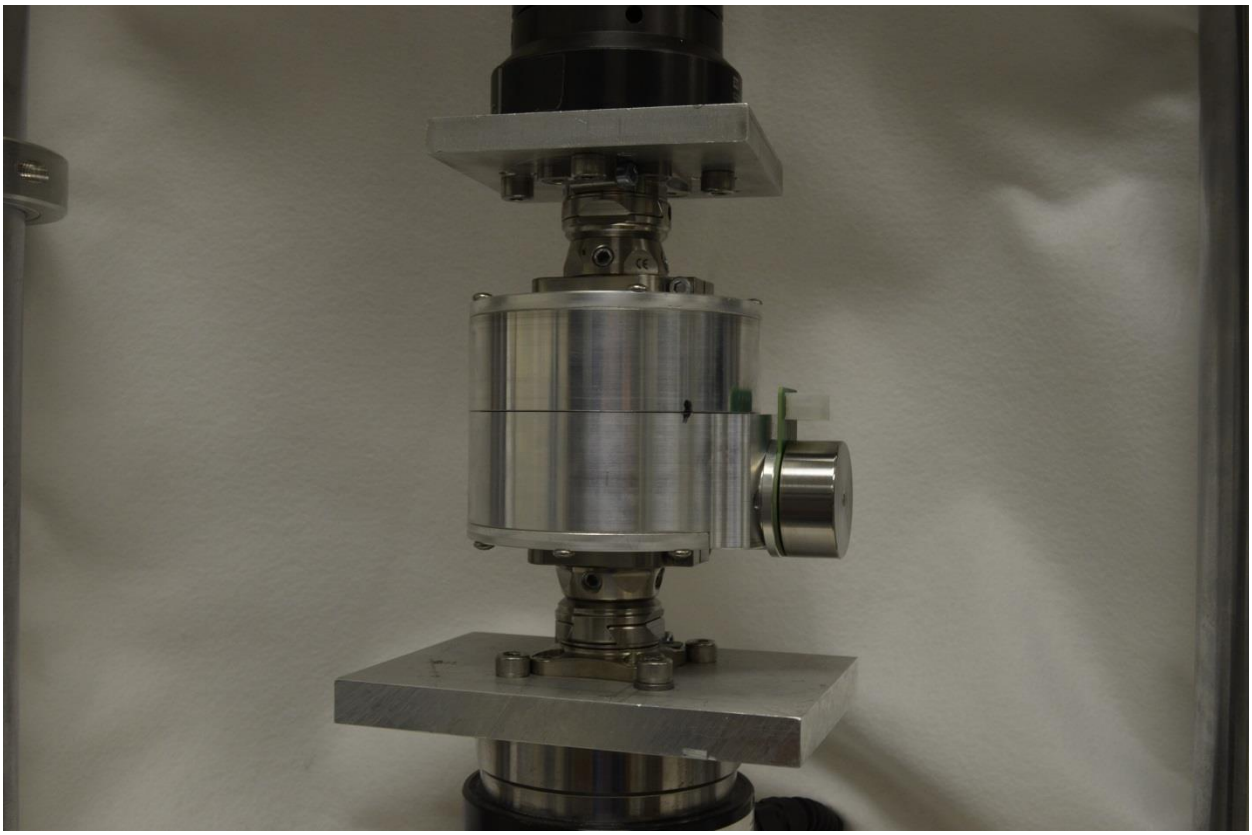

Figure 27: VSTA fixture on MTS for torsional bench testing.

Similar to the spring testing the VSTA was run through its full range of motion (+/- 30°) at both 0.5 °/s and 60°/s. Testing on the VSTA was done at four static stiffness setting: 0.10, 0.33, 0.64, and 1.17 Nm/°. These settings represent the minimum and maximum stiffness capable by the VSTA. The stiffness of 0.64 Nm/° represents a mean value of other devices currently on the market, and the 0.33 Nm/° represents the 1:1 (spring deflection : device deflection) ratio of the VSTA which was useful to evaluate any effects the VSTA might have over the torsional spring alone. After testing was complete, the VSTA was evaluated with no spring using the same test procedure to characterize friction.

3.2.2 VSTA Bench Testing Results

Testing was separated into the four categories of direction and load rate (CW, CCW, 0.5°/s, and 60°/s). Data from each set of trials was then compared to the predicted model. Each

condition was a combination of speed and direction denoted in the figures as clockwise (CW), counter-clockwise (CCW), 0.5 °/s, and 60 °/s. The settings for the stiffness of the VSTA are noted both by the modeled stiffness and the distance of the slider from the spring pivot (Spring Offset, Figure 11). The farther the slider is from the pivot, the lower the stiffness of the VSTA. The relationship between the VSTA stiffness and the position of slider is shown in Table 6.

Table 6: Correlation between VSTA stiffness and position of slider in relation to lever arm pivot.

Stiffness (Nm/°)	Offset from Pivot (mm)
0.10	38.10
0.33	20.64
0.64	14.17
1.17	9.53

Data from the following four charts shows results from the individual stiffness settings for the VSTA. Each condition was run for three trials which were found to have less than 1% variation between trials, with a maximum of 3.5% variation between trials at the 1.17 Nm/° setting (Figure 28), the cause of which is discussed later. Because of the consistency between the three trials, data at each of the four conditions consists of the combined data from the three trials at each condition. Figure 28 depicts VSTA testing at the highest stiffness setting of 1.17 Nm/°. It can be seen from the chart that there good consistency between all four conditions shown.

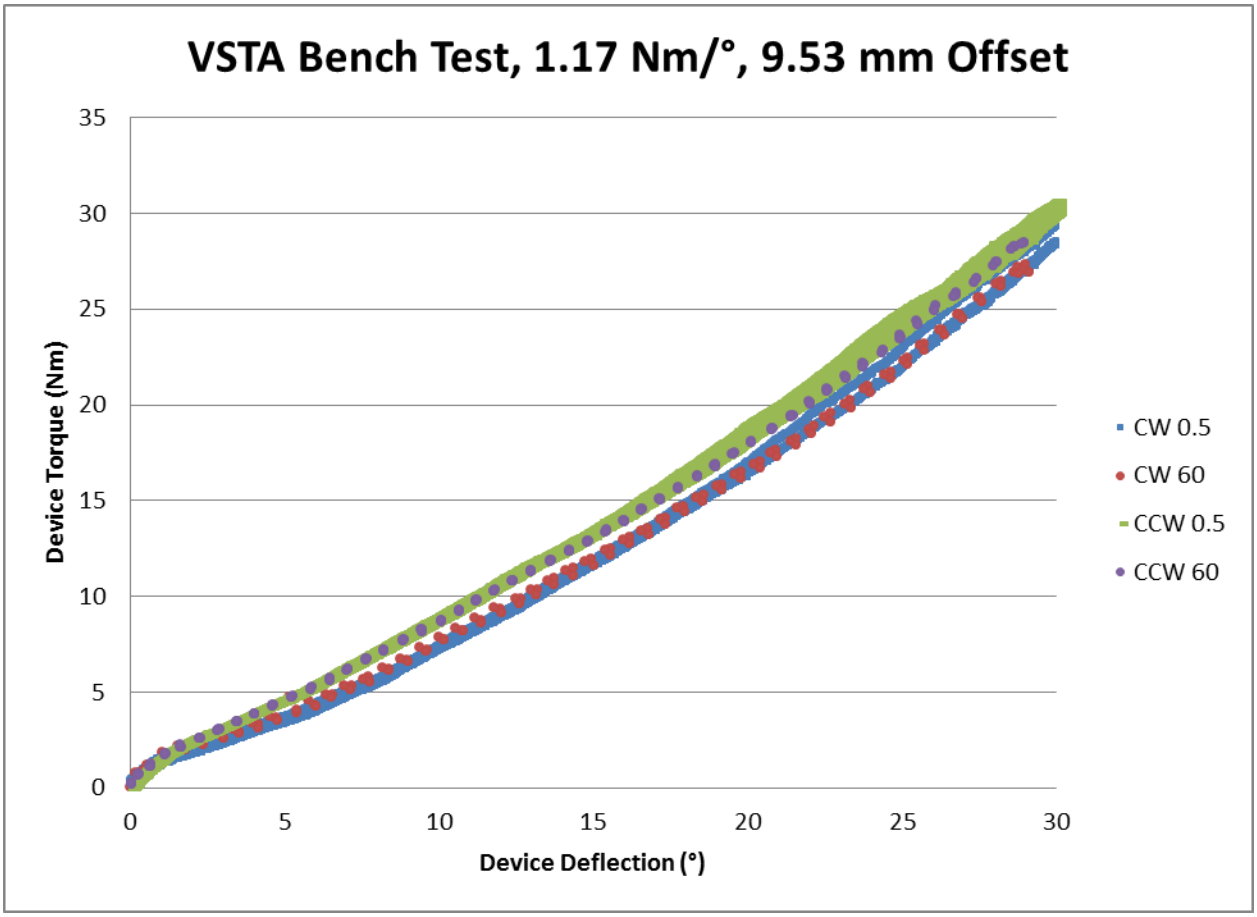

Figure 28: VSTA test at 1.17 Nm/°, 9.53 mm offset from pivot.

Data from the 0.64 Nm/° setting, is seen to be highly linear and have excellent consistency between conditions, Figure 29.

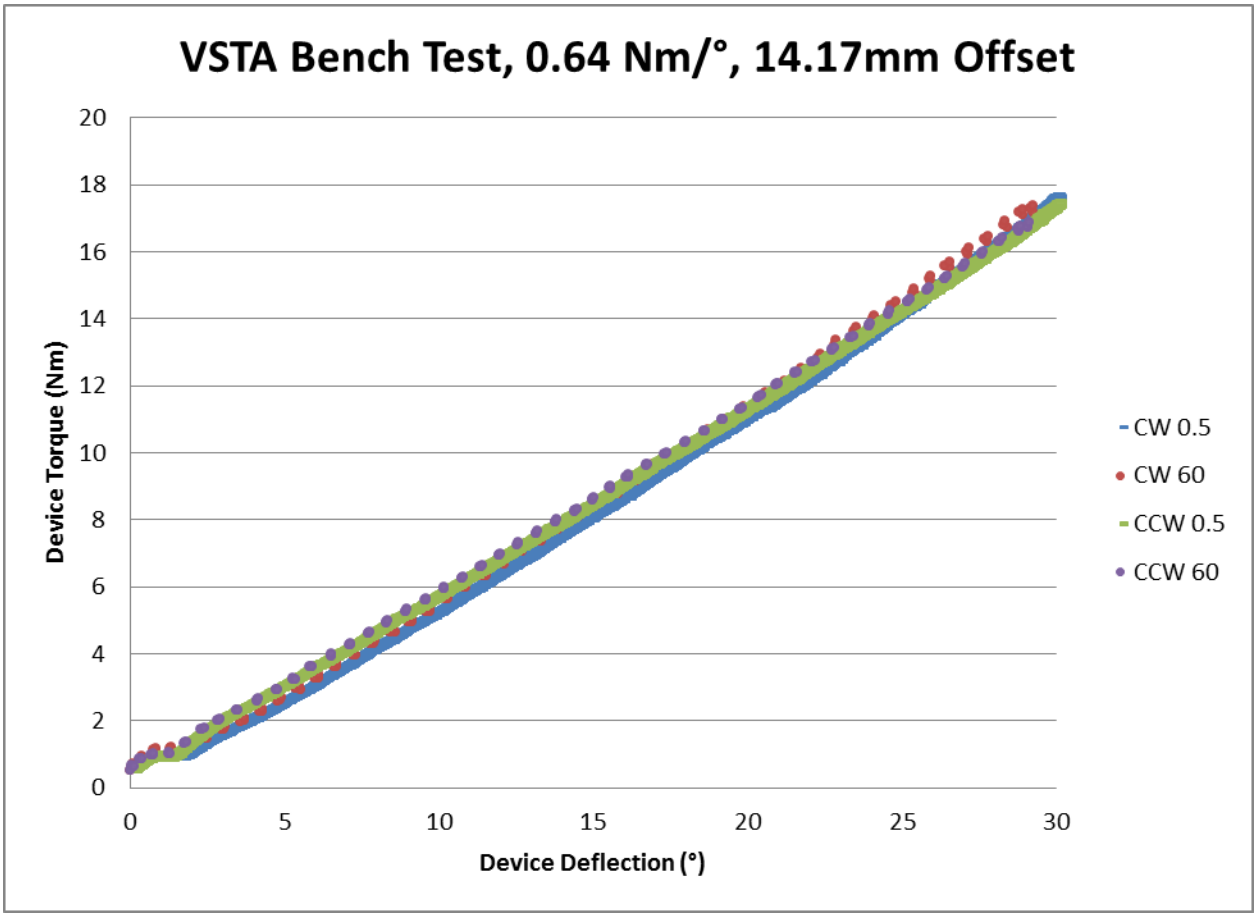

Figure 29: VSTA test at 0.64 Nm/°, 14.17 mm offset from pivot.

Results from the 0.33 Nm/° VSTA setting are also linear and consistent, Figure 30. The 0.33 Nm/° setting represents the 1:1 setting of the VSTA which is reflected in the rate of the VSTA equaling the rate of the internal torsion spring.

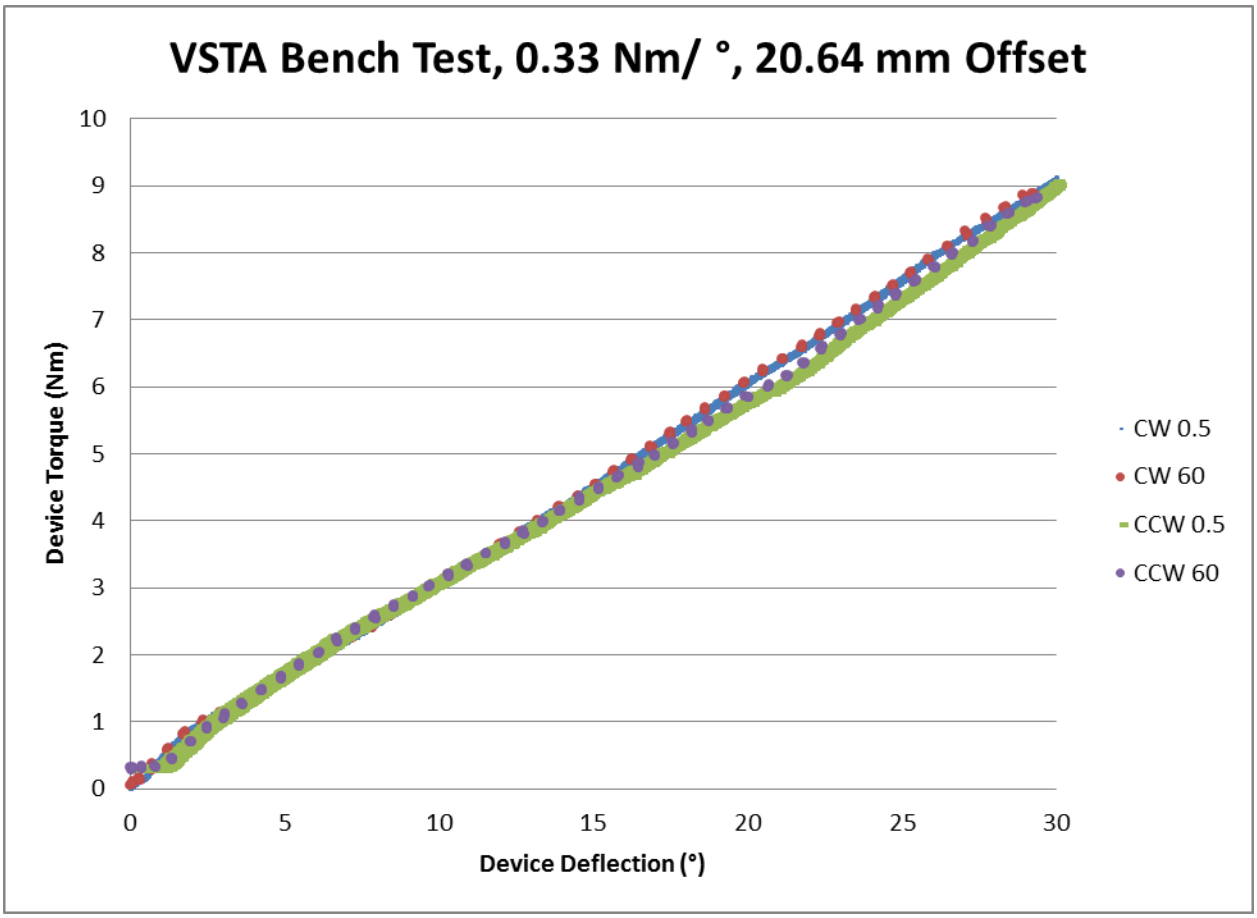

Figure 30: VSTA test at 0.33 Nm/°, 20.64 mm offset from pivot.

Data from the lightest setting available to the VSTA is also highly linear and consistent, Figure 31.

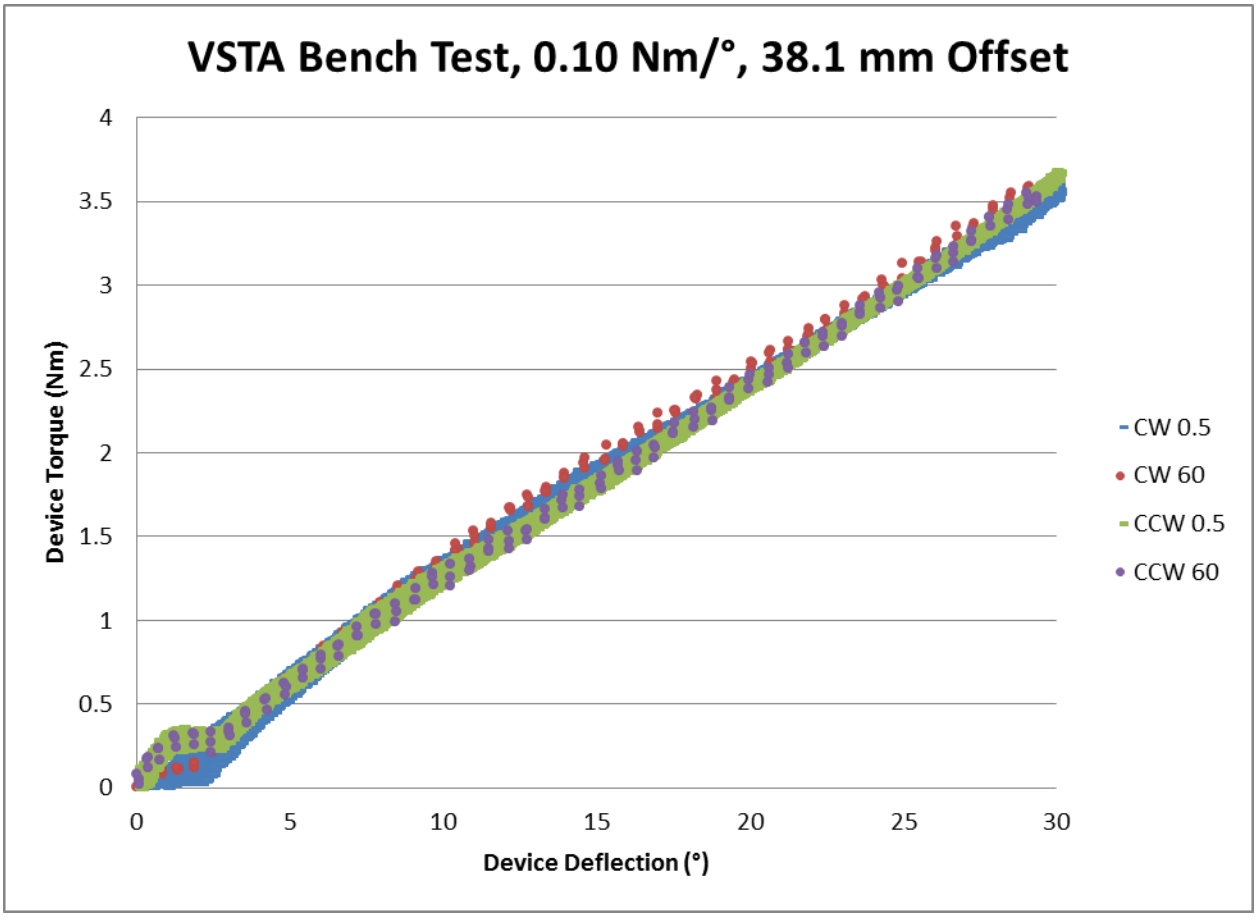

Figure 31: VSTA test at 0.10 Nm/°, 38.1 mm offset from pivot.

Comparison values for each of the four preceding graphs are compiled in Table 7. Similar to the spring testing, this information is important when evaluating if direction or displacement rate play a role in the performance of the VSTA. The table shows comparisons of the VSTA rate, between tested conditions, which was determined for each condition via a linear fit trend line forced through the origin. It can be seen in the table that generally the direction and speed of deflection does not greatly influence the measured rate of the VSTA. One exception was for the 1.17 Nm/° setting, which is discussed later.

Table 7: Comparison of VSTA performance at each stiffness setting

		Percent Difference (%)			
	Comparison	CW: 0.5 vs 60	CW 0.5 vs CCW 0.5	CCW: 0.5 vs 60	CW 60 vs CCW 60
VSTA Rate (Nm/°)	1.17	0.35%	7.99%	0.81%	9.15%
	0.64	-1.33%	0.95%	0.35%	0.02%
	0.33	-0.11%	0.72%	0.23%	0.60%
	0.1	-0.34%	0.02%	0.07%	0.43%

Using the results at the individual stiffness settings, a comparison could be made between the actual VSTA performance and the model predictions, Figure 32. In the figure, the data from the four separate conditions (CW, CCW, 0.5 °/s, and 60 °/s) are combined as a single data set. Each data set is then given a linear fit, forced through the origin, to determine the actual spring rate achieved by the VSTA. This value, along with the goodness of the fit, are shown adjacent to each data set in Figure 32. It can be seen in the figure that at the lower stiffness settings, the VSTA matches well to the model prediction. However, at the highest stiffness level, there is a significant deviation between the VSTA actual performance and the model. A summary of the data presented in Figure 32 along with an analysis of how it compares to the model is given in Table 8. The data in the table tabulates how much the VSTA actual varies from the model, as well as showing how well the linear trend line fit the data. The percentage of deviation is calculated by determining the difference in rate between the model and actual and representing that deviation as a percentage of the total stiffness range of the VSTA. It can be seen for the lower three stiffness values that the VSTA differed by less than 10% from the model prediction, the large deviation of the 1.17 Nm/° setting is discussed later. The linear fit numbers show the R^2 values of the linear trend lines to the data. This indicates that the linear fit is an excellent approximation of the actual data, and that the response of the VSTA can be taken as linear.

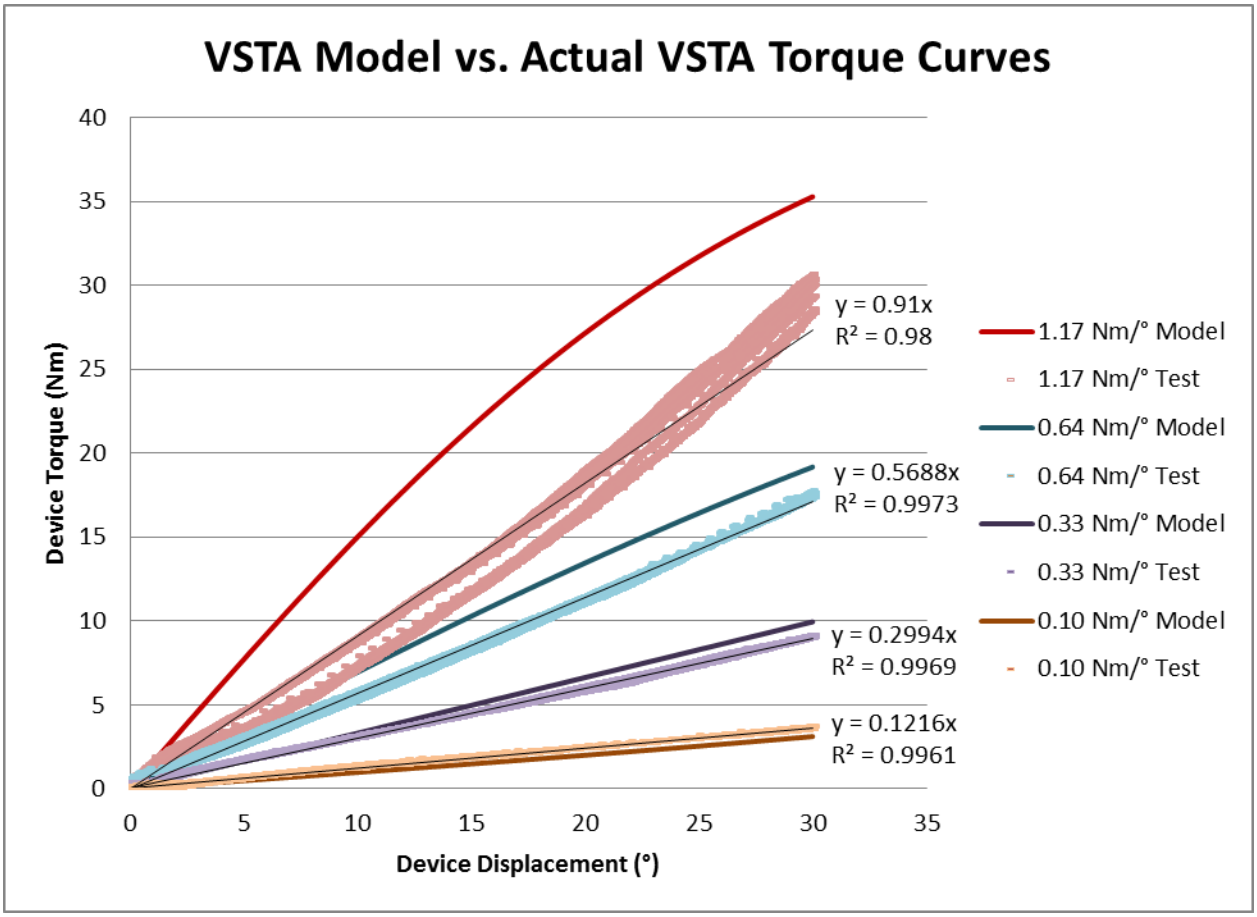

Figure 32: VSTA Performance as compared to VSTA Model

Table 8: Analysis of VSTA data in comparison to model predictions.

Modeled Stiffness (Nm/°)	VSTA Stiffness (Nm/°)	Deviation from Model as Percentage of Full Stiffness Range	Device Fit R^2 (Linearity of Results)
1.17	0.91	24%	0.978
0.64	0.57	7%	0.997
0.33	0.3	3%	0.997
0.10	0.12	2%	0.996

Lastly, the VSTA was run through the same set of tests as previous, but with no spring installed, to quantify any friction in the system. It was found that the frictional effects of the VSTA with no spring were less than 0.25 Nm, and so deemed inconsequential.

Using the data gathered, a plot of the VSTA stiffness was made in relation to the Spring Carrier position relative to the Lever Pivot, Figure 33. This plot is interesting as it shows the sensitivity of the position of the spring carrier in relation to the desired stiffness. The plot also shows the deviation of the actual results from the model at higher stiffness values. Figure 33 uses a power curve to establish the relation between the spring position and the stiffness. This curve could later be used to establish a controller for the motor on the VSTA to command the position of the spring in order to obtain a specific stiffness, or a stiffness profile.

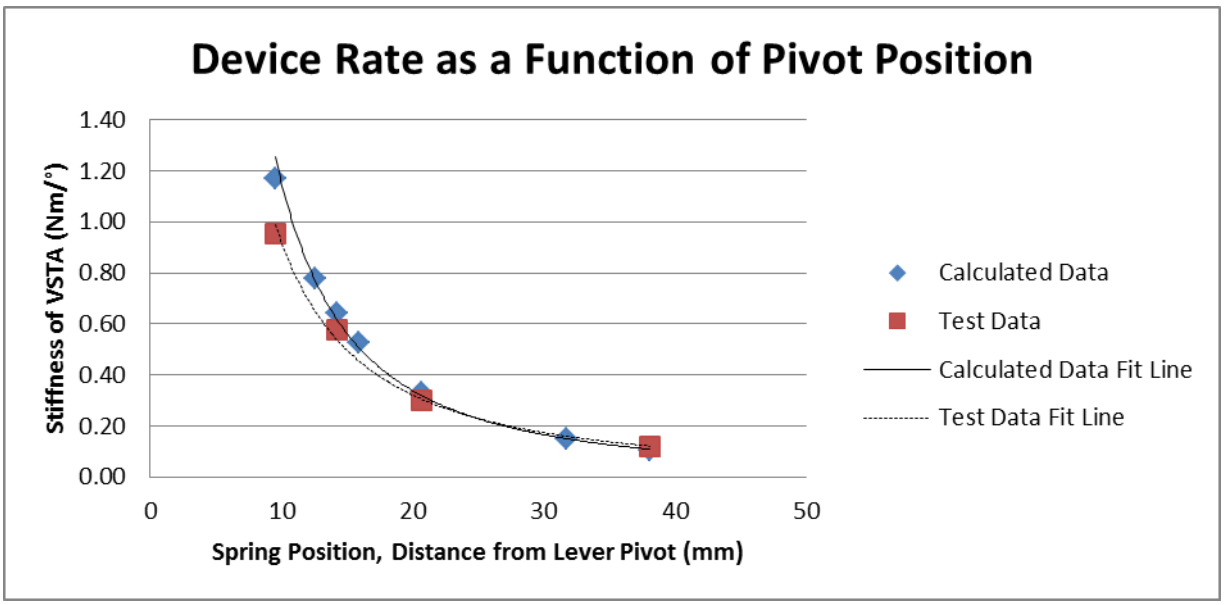

Figure 33: VSTA Stiffness as a function of Spring Carrier position in relation to the lever Arm Pivot

The final physical attributes, as compared to the initial design goals, can be found in Table 9. It can be seen in the table that the stiffness range of the VSTA is slightly reduced from the model predictions, but still maintains a maximum stiffness greater than devices currently on the market. The mass of the VSTA is also slightly larger than the computer model predicted, but this is to be expected as the final prototype does not follow the original design exactly, as discussed previously.

Table 9: Comparison of initial design and final specifications of the VSTA

	Motion Range	Stiffness Range	Mass	Size
Initial Design	±30°	0.10-∞ Nm/°	1.27 Kg	89 mm tall x 111 mm Dia
Final Implementation	±30°	0.12-0.91 Nm/°	1.56 Kg	89 mm tall x 111 mm Dia

3.2.3 VSTA Testing Analysis

Similar to the spring alone test, the VSTA testing exhibited negligible difference in performance between the 0.5 and 60 °/s speeds and the clockwise and counter-clockwise directions, so all data was grouped together. There was an exception for the 1.17 Nm/° data which varied up to 9% between clockwise and counter clockwise due to internal deflection which is discussed later. The grouped results of the VSTA test were fit using a least squares optimization to determine the effective stiffness of the VSTA at the individual settings. The actual tested stiffnesses of the VSTA were then compared to those modeled (see Table 8). The goodness of the linear fit of the test data is indicated by the accompanying R^2 values.

It was found that at the lower stiffness settings, the model and VSTA experimental results matched closely, with deviation from the model less than 10% of the full scale VSTA stiffness span. However, at the 1.17 Nm/° setting, there was a large deviation from the model, as well as less consistency in the repeatability of the VSTA. An investigation into the inconsistency found that at the higher stiffness setting, the VSTA experienced significant internal deflection of the spring carrier along the guide rails. This was a result of the higher forces on the top of the spring post from the lever arm, and the large moment arm that this induces over the bottom of the carrier at the guide rails, Figure 34.

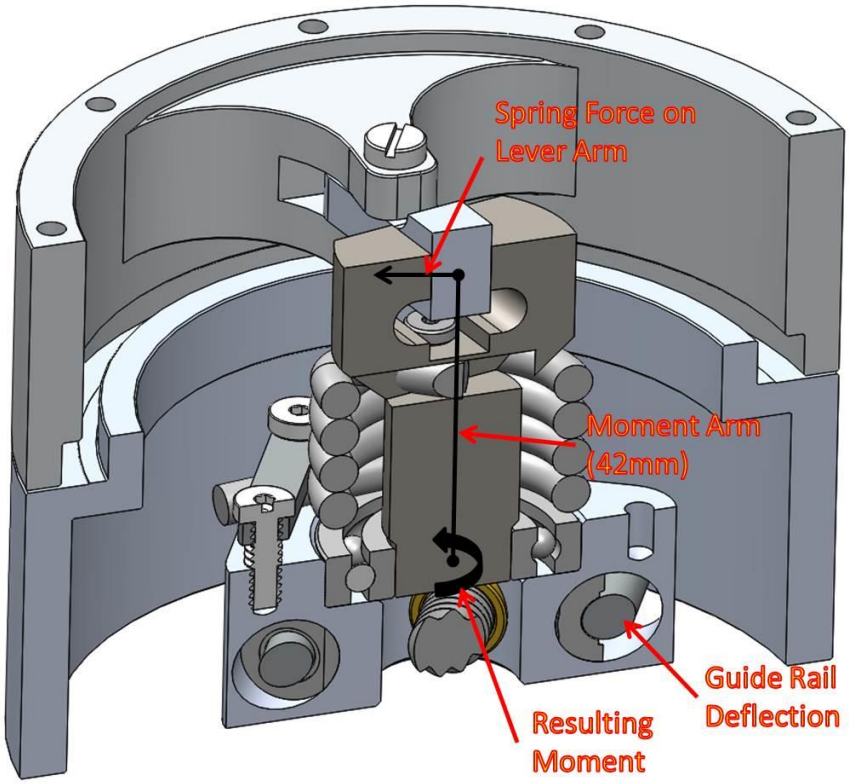

Figure 34: Illustration of forces resulting in large internal deflections at high stiffness settings.

This deflection is a design issue that could be resolved by working to reduce the length of the moment arm and relocating the spring. This deviation is only an issue at the highest stiffness settings and while it is not congruent with the model, the response of the VSTA is still linear, and predictable given the test data. Another consideration is that the peak torque for a turning amputee has been recorded to peak around 11.8 Nm, which would be approximately 12° of deflection at the 1.17 Nm/°, less than half the functional range of the VSTA, minimizing the internal deflection [18].

The VSTA is infinitely variable within its stiffness limitations; however, the resolution to achieve the stiffness values in relation to the carrier position is highly non-linear. Figure 33 shows how the stiffness of the VSTA can be varied through that range by positioning the Spring Carrier, with the trend of the VSTA accurately fit by a power curve (R^2=0.998). This indicates

that for active control of the VSTA, a controller could be easily programmed with the curve to accurately assign stiffness profiles to motor positions. A discussion of these results follows.

3.3 Bench Testing Discussion

Results from the bench testing show that the VSTA is a viable device to demonstrate whether variable transverse plane stiffness would be of benefit to a lower limb amputee. Bench testing methods were modeled to conform with Flick et al. [18] and so comparisons to the single stiffness devices tested can be made. It was found that the VSTA was not rate dependent, performing equally well at 0.5 °/s and 60 °/s. The VSTA was capable of stiffness infinitely variable between 0.12-0.91 Nm/°, with a movement range of +/- 30°. This exceeds the capabilities of the single stiffness devices tested by Flick et al., which generally peaked around 0.7 Nm/° [18]. The maximum stiffness range of the VSTA corresponds to a maximum torque capability of 27 Nm, also in excess to the capabilities of the intact human ankle. At the maximum stiffness setting of 0.91 Nm/° and a deflection of 15°, the torque in the VSTA would be 13.65 Nm, comparable to the 11-12 Nm maximum at 15-20° found in the intact human ankle [18], [28]. Lastly, testing of the VSTA at its 1:1 (spring deflection : device deflection) ratio demonstrated that it does little to modify the dynamic response of the internal spring, resulting in a predicable linear response from the VSTA. It is unknown if a linear torque response is optimal, but a nonlinear torque response [18] could be achieved by the VSTA by varying the stiffness in real time.

The VSTA is a prototype, and as such has limitations. The current VSTA prototype is limited to stiffness changes under no load (swing phase), precluding the ability to create custom torque curves by actively adjusting the pivot position while under load. This also limits the VSTA to operation as a state machine, with single stiffness settings applied to single tasks such as turning, pivoting, or walking. Another limitation of the current VSTA layout is its inability for infinite ratio variation between the minimum and completely stiff values. Lastly, Figure 33

shows a significant reduction in position resolution as the stiffness increases. This means that as the stiffness increases, the position controller must become increasingly more accurate in order to hit a specific stiffness value. This curve could be modified in the future by developing a spring with a higher stiffness value, effectively skewing the trend to the right, and providing more resolution at the higher stiffness levels. These shortfalls will be addressed in future iterations of the VSTA in order to achieve the maximum utility, with no risk of damage due to over stress of the spring, and reducing internal deflections.

3.4 Bench Testing Conclusions

The VSTA is capable of varying its stiffness between 0.12-0.91 Nm/° with +/- 30° of rotational motion, and also includes a mode for fully locked operation. The VSTA performs this function by varying the mechanical advantage between the housing and an internal torsion spring via a lever with an adjustable pivot point. This technique for stiffness variation allows for infinite stiffness variation within the operating range. Also, because changes in stiffness are not performed by direct changes to the spring deflection, the variations can be done by a low torque electric motor saving energy and weight. The VSTA as tested matched closely with model for its performance, however, at higher stiffness levels deflection of the internal components was found to occur resulting in a deviation from the expected behavior.

4 VSTA Control System Testing

A simple control system for the VSTA was developed and tested. As previously discussed the VSTA will initially be used as a state machine, such that single stiffness settings will be used for individual tasks. This type of operation only requires simple position step commands for a controller. To perform this operation, a proportional-integral-derivative (PID) controller was used to modulate the position of the motor to achieve changes in the spring carrier position resulting in a change to VSTA stiffness.

4.1 Controller Testing Methods

A Maxon controller, EPOS 24/5 (PN 275512 Maxon Motor AG, Switzerland), and control software, EPOS Studio (2.0, Revision 2), were used to perform the stiffness selection task. The EPOS 24/5, limited to 24 volts and 5 amps maximum, allowed for direct control of the motor via an RS232 to USB computer connection, while the EPOS studio uses a PID control scheme for step position control. The position of the EC 45 motor was monitored via the three internal Hall effect sensors. While using a Hall Effects sensor for motor position is less ideal than an encoder, or linear potentiometer on the carrier, the motor manufacturer indicates that it is sufficient for motors with greater than four pole pairs. The EC 45 has eight pole pairs.

The control employed by the EPOS Studio utilizes parallel PID control (Figure 35) with a sample rate of one kHz, however, recording was limited to 512-bits that was then divided between the channels due to the serial sampling of the software. Three of the four channels were 32-bit, and one was 16-bit, which only allowed for 72 samples over the 2 second period, resulting in a 36 Hz sample rate.

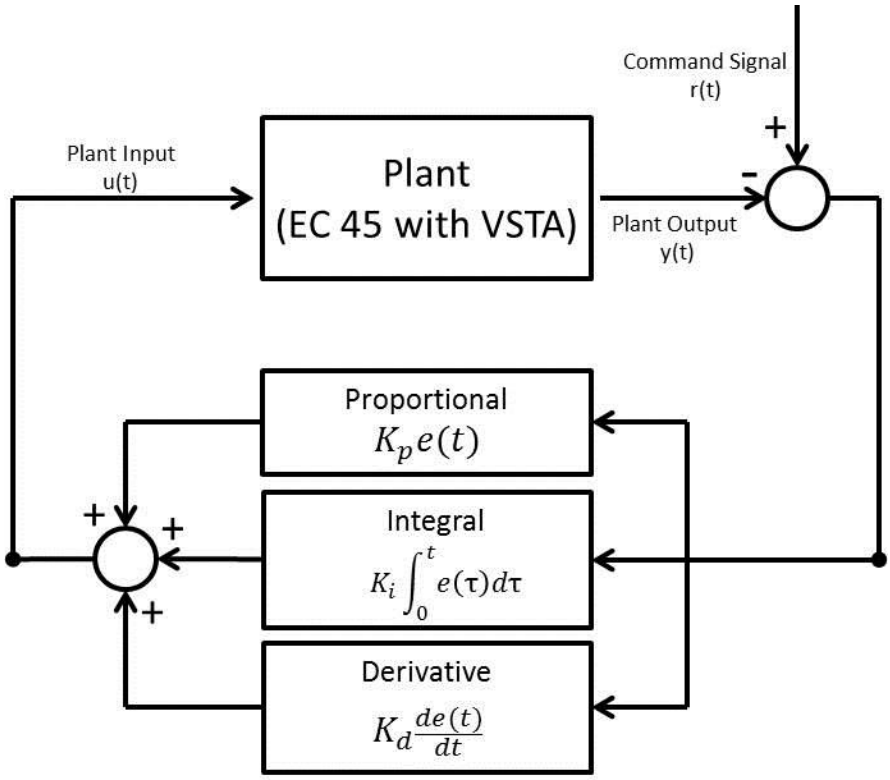

Figure 35: PID Control Diagram

While the EPOS Studio software comes pre-loaded with suggested gains, it was found that these gains resulted in an unstable system. Specifically, when commanding a step input, the controller would command a ramp at too high a rate, causing a motor fault state. Preliminary tests revealed that the 24 volt supply, coupled with large step input commands, resulted in excessively high current requirements. It was found through trial and error that 16 volts was the maximum supply that could be reliably provided without tripping an excess current fault. Additionally, efforts to use the EPOS Studio auto tune function alone to optimize gain settings did not produce a sufficiently fast response with limited overshoot and oscillation without exceeding motor fault limits. Due to these factors, the PID gains were set manually after utilizing the auto tune function to set base values.

The tests run on the control system of the VSTA were done with Kp, Ki, and Kd set at 10,000, 75, and 20,000, with a supply of 16 volts. These values for the PID gains, while not

optimal, were able to get a fast response at the lower supply voltage while minimizing overshoot and ringing. This process resulted in Kp and Kd values much greater than expected. The Kd value might normally be kept at a far lower value to minimize interference from signals with rapidly changing values with respect to time, such as noise. However, for this case, it was found that increasing the Kd value did not have any detrimental effects, proving useful in minimizing overshoot and nearly eliminating oscillations.

Tests were run for eight step inputs to the VSTA of varying size (38.1, 28.57, 20.64, 14.17, 11.11, 9.53, 6.47, 4.64 mm). This was done to best characterize response the system would have to different stiffness requirements. Ranges included the full stiffness range of the device from fully locked to the minimum stiffness position, as well as all the ranges between the five previously tested stiffness positions. Each trial recorded the actual motor position, position command, average actual motor speed, and average actual motor current. The first two variables were chosen to help evaluate if the VSTA was positioning accurately, and how quickly it was able to make the position change, the second two were used to evaluate how the controller was conducting the step change.

Response curves were evaluated for the following characteristics, and calculated as follows: Rise Time is calculated as the time between 5% and 90% of the steady state value; Percent Over Shoot is the percent of the steady state value that the curve achieves at its maximum; Settle Time is set from the step command until the curve settles to within 5% of the steady state value; and Steady State Error is the difference between the command and the final steady state value of the response curve. For the purposes of this project the Settle Time and Steady Stat Error are the most important values as this indicates how quickly and accurately the controller was able to set the stiffness of the VSTA.

4.2 Controller Testing Results

Results were recorded for each of the eight step tasks. Figure 36 shows an example of the VSTA control response for a given step input. Only one full graph is shown as all additional tests exhibited the same information relative to the size of the step command.

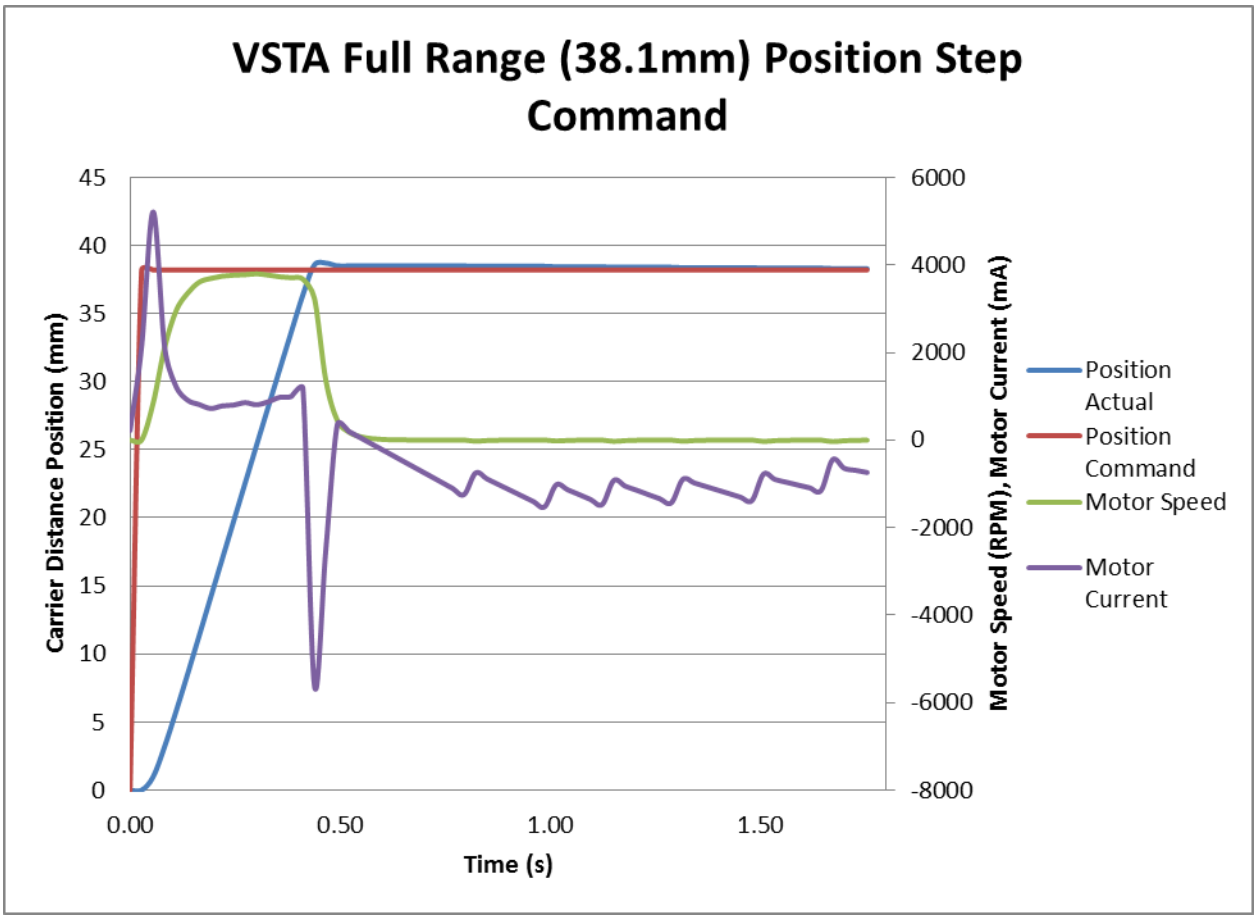

Figure 36: Recorded control response of the VSTA during a sweep of the full motion range (38.1mm, Full lock to 0.12 Nm/°)

The system responds quickly to step input and achieves the commanded position with a an overshoot of 1.06%, a single oscillation, setting in 0.47 s at maximum, Figure 36. This is a factor of the high Kd gain that was described previously. It can also be seen that the motor current quickly reaches the five amp limit that forced the reduction of the input voltage from 24 volts to 16 volts. Motor speed can also be seen to be very stable during the transition, reaching a peak of around 4000 rpm in 0.30 s. A simplified model calculation relating the motor power

(current times voltage) and the mechanical power (torque times angular speed of the motor) shows that at the 3778 rpm, 5.2 amps, 16 volts, the motor is producing 210 Nmm of torque. Referencing the datasheet for the EC 45 [35], this is congruent with the maximum speed, current, and torque conditions. However, if the motor was allowed to run at the full 24 volts more power would be available for the step command. Torque could be increased, helping to decrease the time required to make the position movement, and will be addressed later in the results and discussion.

The results for six of the eight individual step command, and system responses are shown in Figure 37. Two of the results, as well as the velocity, and current data were left off of the chart to enhance readability.

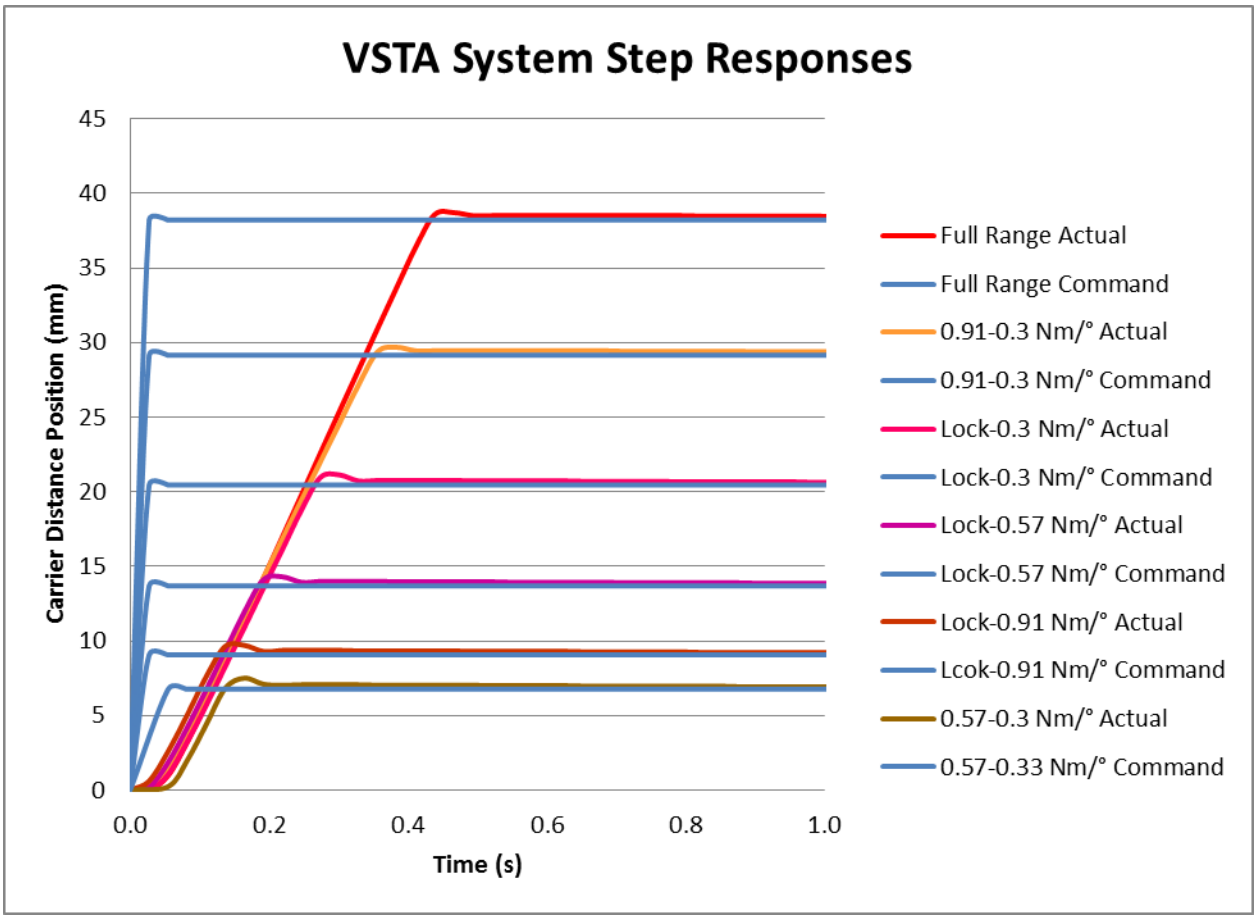

Figure 37: Step input responses for VSTA position commands of varying lengths

At a maximum the VSTA took 0.47 seconds to move from fully locked to the minimum stiffness position for 0.12 Nm/°. The steady state error was found to be very low at 0.03-0.1 mm, a value that is of no consequence to the system. The 0.47 second time is the largest concern, as the target time was to be less than 0.25 seconds to fit within the swing phase of the average human gait [34].The step response was very consistent for the varying step sizes. Each with similar rise rate, little overshoot, negligible oscillation, and little to no steady state error. Data for these tests is compiled in Table 10.

Table 10: VSTA Controller Step Response Data

Test	Dist Traveled (mm)	Rise Time (s)	Percent Over Shoot (%)	Settle Time (s)	Steady State Error (mm)
Full Range	38.1	0.33	1.06%	0.47	0.1
0.91-0.1 Nm/°	28.57	0.22	1.05%	0.38	0.1
Lock-0.3 Nm/°	20.64	0.2	2.97%	0.33	0.07
Lock-0.57 Nm/°	14.17	0.15	3.93%	0.25	0.07
Lock-0.91 Nm/°	9.53	0.11	6.30%	0.19	0.07
0.91-0.3 Nm/°	11.11	0.11	6.78%	0.19	0.07
0.57-0.3 Nm/°	6.47	0.08	9.90%	0.16	0.07
0.91-0.57 Nm/°	4.64	0.08	10.14%	0.16	0.03

One way to improve this is to modify the controller to allow for the full 24 volt supply to the motor. Further tests were performed in which the motor was supplied with 24 volts and run through the full range of 38.1 mm and the half range of 20.6 mm. For these tests the motor was deactivated into fault mode before the step could be completed. It was found that for the full range, 24 volt attempt; it took 0.34 s from the step command until commanded position was passed. Assuming that the motor could be controlled similar to the 16 volt trial, which took 0.05 s to settle to the set position from the time it initially overshot the command, it is estimated that the VSTA is capable of 0.39 s for a full range stiffness variation. A 24 volt attempt was also performed for the half range step, which took 0.18 s to initially overshoot the command. Using a similar extrapolation it is assumed the VSTA is able to attain 0.23 s for this step size at full

power. These values are more in line with the requirements of the VSTA, and would allow more capability in future testing.

4.3 Controller Testing Discussion

Testing of the controller and motor of the VSTA was completed for a step input response congruent with use of the VSTA as a state machine. The VSTA had acceptable response for position accuracy, and was able to move relatively quickly. Initially, the results indicate that the VSTA step response will not be fast enough, even if it is run at the full 24 volts. However, at this time there is no data to indicate what stiffness values might be required for varying activities, and so no estimation can be made to predict if the full range step command will ever be necessary. Additionally, it should be noted that the full range of the VSTA stiffness capability might not even be usable as it is able to attain stiffness values as low as 0.12 Nm/°, well below the minimums of devices currently on the market, which only go as low as 0.5 Nm/° [18]. Using this fact conservatively, allowing that the VSTA might have useful range as low as the median value of 0.3 Nm/° up to completely stiff, the VSTA should have the capability to sweep the range in 0.23 seconds, meeting the original goal. Another consideration is that changes in stiffness that do not originate, or end in the completely stiff position will have considerable less distance to travel. Referencing Table 10, it can be seen that even with the 16 volt supply, the VSTA was able to sweep the usable range from 0.91-0.3 Nm/° in 0.19 seconds, well within the 0.25 second goal. Additionally, the step command that was required during this project was a worst case scenario for the VSTA. Continued testing might show that a more gentle sloping command might allow for more smooth transitions at higher voltage supplies, while only adding small amounts of time to the predicted responses.

Another consideration for enhancing the performance of the VSTA would be to optimize the PID gains of the control system, or devise a more efficient control system completely. This

could be done by starting with the system as a whole, generally an electric motor system can be characterized by:

$$J\ddot{\theta} + b\dot{\theta} = Ki \tag{10}$$

$$L\frac{di}{dt} + Ri = V - K\dot{\theta} \tag{11}$$

Equations 10 and 11 can be formatted into a state space or frequency domain model which would then allow for offline optimization of the system, and possibly a faster system. However, at this time there is not enough data on the system to accurately complete the model. While the moment of inertia (J) of the motor and armature constant (k) are known from the manufacturer, the additional component for J from the components of the VSTA would have to be measured, as would the damping coefficient 'b' composed of the friction and load of the VSTA components.

The VSTA controller is used to achieve step changes in position of the spring carrier, and so it must be noted that this does not linearly correlate to the stiffness settings of the VSTA. Referencing Figure 33, the relationship between carrier position and VSTA stiffness can be seen to be related by:

$$Stiffness = 30.35x^{-1.519} \tag{12}$$

Where the distance 'x' in equation 12 is measured from the completely stiff position and fit the measured data with an R^2 value of 0.9976. As previously discussed, the useful range of the VSTA is in a relatively small portion of its overall range. While this was presented as a possible drawback of the VSTA's ability to resolve different stiffness in the useful range, it can be seen as a benefit to allowing fast stiffness variations by reducing the size of step changes. In order to fully implement control of the VSTA, a position sensor would be required in order to indicate VSTA deflection, which could then be related to torque in the joint. This information would be crucial for understanding VSTA performance and operation when being used in future human testing. While the addition of this sensor is critical to successful field testing of the VSTA, it was

negated for this level of the project as measurements of deflection were otherwise accounted for in the lab via the use of the MTS machine, and the infrared camera system for later human subjects trials.

4.4 Controller Testing Conclusions

This section presented a PID control scheme to allow for step position changes, congruent with the use of the VSTA as a state machine. It was shown that the VSTA PID controller could accurately attain any position in the range required by the VSTA. The controller did lack the speed necessary to sufficiently meet the initial goal of 0.25 seconds for a full range sweep, however, it was estimated that if the controller could have been run at the full 24 volt supply, and the actual usable range of the VSTA was considered, the controller settling time was more than sufficient to make changes to the stiffness during the swing phase of the average amputee's gait.

5 Future Work

Initial tests on the VSTA demonstrate its acceptability for human subject testing. Improvements to the system to enhance its function include structural improvements to ensure robust function in all types of situations. Furthermore, the ability to sweep the entire stiffness range from the minimum to completely stiff, as well as the ability to change stiffness actively while under load needs to be addressed. The control scheme should be updated using a full model, and a controller identified that can achieve the full capabilities of the system. Additionally, human testing needs to be performed in order to evaluate the actual functionality. Human subjects testing will also provide insight as to the benefit of variable stiffness in the transverse plane.

5.1 VSTA Improvements

The VSTA's functionality has been shown to be acceptable, but as noted previously, some compromises were made during design and fabrication. Structurally the VSTA was deemed acceptable for initial testing, however, with a factor of safety of less than two on multiple components. The structure should be increased to ensure the ability for longer term testing without risk of failure. Additionally, as illustrated in Figure 34, the internal function of the VSTA should be revised to reduce deflection of the internal components.

Another limitation of the VSTA is the inability to vary the stiffness infinitely between the minimum and completely stiff. This feature was limited by the maximum spring stress encountered at higher stiffness settings. This could be avoided by designing and sourcing a spring with a higher rate. A higher spring rate would limit the deflection required to reach higher stiffness settings, and reduce spring stress.

Another possible improvement to the VSTA would be individual springs for clockwise and counterclockwise motion. During mechanical testing, it was found that deflecting the single spring against the wind direction resulted in higher spring stress, as well as load profile, while having the same overall linear stiffness, had a noticeably different load profile than deflection with the coil wind. Other benefits of a two spring system is the ability to differentiate the spring stiffness's for the different direction of rotation, which could prove beneficial as the stiffness of the intact human ankle does not necessarily exhibit symmetric stiffness [28]. Lastly, individual springs would allow for preload to be applied inside the VSTA to eliminate free play around zero deflection. Anecdotally, when examining the VSTA in the laboratory, it seemed loose around zero deflection. This could be eliminated with a small amount of preload not available to the single spring setup.

Lastly, the VSTA should be evaluated for its ability to actively change stiffness during the stance phase of gait in order to create custom stiffness profiles. While this is not a requirement

of the project currently, it has been suggested that the stiffness of the human ankle is not strictly linear, and such the VSTA should be tested and modified to accommodate this [17, 18].

These modifications, while ideal, would need to be balanced against increases in size and mass that might result from increasing spring size, or adding additional components.

5.2 Control System Improvements

As previously discussed, the controller could be improved by allowing the VSTA motor to operate at the full 24 volt supply. Additionally, a model for the entire system could be made to optimize the control gains, or design a new control scheme entirely that might allow for faster, more efficient step changes. Future versions of the controller should allow for the use of active position control that would be capable of a variable stiffness profile executed over the entire gait cycle as opposed to a static stiffness setting for each step. While the VSTA will initially be used as a state machine, it may become necessary in the future to create custom stiffness profiles during the stance phase of gait by actively manipulating the position of the spring carrier while the VSTA is under load. Another improvement will be to include the controller and power supply as an onboard package. Currently, the VSTA is tethered to a desktop voltage supply and laptop, but more extensive testing will require a standalone setup. The control system as it is currently is sufficient for initial laboratory testing, however, the issues of a more powerful, and optimized controller should be addressed before any stand-alone field testing is attempted.

5.3 Proposed Human Subjects Testing

To properly evaluate the function of the VSTA, human subject's testing should be performed. The aim of such tests would be to determine if variable torsion in the transverse plane might be of some value to an amputee performing activities encountered in everyday life.

Specifically, the VSTA should be tested in a way that best replicates maneuvers that are encountered in everyday life.

It has been shown that everyday ambulation can be composed by as much as 50% turning steps [11]. Turning steps are of key importance to testing the VSTA as this type of maneuver induces greater transverse plane moments, as well as range of motion [36]. Tests that might be considered would be measurements of self-selected walking speed which has been related to overall gait stability [37]. The timed up and go (TUG) test is a standard clinical test that could be used to test overall mobility; however, it only includes a single 180° turn and has been shown to have ceiling effects for healthy walkers, and may not provide enough variation to properly evaluate the VSTA [37, 38]. To better test the subject's ability to ambulate successfully with the VSTA, a modified version of the TUG known as the L-Test of functional mobility could be used [39]. The L-Test includes both 90° and 180° turns, as well as transfers into and out of a sitting position. The L-Test has also been shown to have a greater ability to distinguish between different amputation types and other mobility impairments [39]. The increased sensitivity of the L-Test would be useful in determining differences in the subjects' ability to ambulate when using different torsional stiffness values of the VSTA. Additional measures of ambulation for comparison during dynamic tests would also include step length [40], and step width [41], which have been used as measures of stability.

Lastly, a static reach test might also be employed. This test would involve the subject reaching for an object at about head height and arm length away while keeping the feet planted. This test might be compared loosely with a static reach test for balance [42]. The aim of the static reach test would be to simulate an activity that amputees might face on a daily basis, such as reaching in the kitchen or garage. This test would look for variations in peak transverse plane moment at different VSTA stiffness settings when twisting to complete the reach. Results from this test would also be of interest in order to decouple the dynamics of walking, with the motion of twisting on the prosthetic limb.

The VSTA as it is presented is suitable for initial human subjects testing in the lab. While it does have limitations both structurally and functionally, as indicated previously, these limitations can be worked around in a monitored, controlled, laboratory setting. This includes use of tethered power and controls, in the absence of an onboard controller and battery. More advanced field testing of the VSTA will require updates to the structural, and functional capabilities of the VSTA, as well as optimization of the controls, and addition of a stand-alone position sensor, and onboard controls and power supply. This would allow the VSTA to fully withstand the rigors of testing outside the lab.

Through human subjects testing, it is hoped to understand more clearly the role of transverse plane stiffness in everyday ambulation. Human subjects testing is also critical to show if the VSTA is effective at producing the results hypothesized earlier, e.g. reduction in soft tissue damage, increasing mobility, and reducing incidents of falls in amputees. Using the tests outlined the VSTA will hopefully show that different stiffness are optimal in reducing peak ankle moments, which would indicate reductions in peak shear stresses in the soft tissues. Additionally, the measures of dynamic stability outlined will show if the VSTA has the ability to increase amputee mobility, as well as helping to increase stability during turns, which in turn could help reduce the instance of falls.

Bibliography

[1] K. Ziegler-Graham, E. J. MacKenzie, P. L. Ephraim, T. G. Travison, and R. Brookmeyer, “Estimating the prevalence of limb loss in the United States: 2005 to 2050,” *Arch. Phys. Med. Rehabil.*, vol. 89, no. 3, pp. 422–429, Mar. 2008.

[2] J. S. Rietman, K. Postema, and J. H. B. Geertzen, “Gait analysis in prosthetics: Opinions, ideas and conclusions,” *Prosthet. Orthot. Int.*, vol. 26, no. 1, pp. 50–57, Jan. 2002.

[3] B. J. Hafner, J. E. Sanders, J. M. Czerniecki, and J. Fergason, “Transtibial energy-storage-and-return prosthetic devices: A review of energy concepts and a proposed nomenclature,” *J. Rehabil. Res. Dev.*, vol. 39, no. 1, pp. 1–11, 2002.

[4] S. W. Levy, “Amputees: Skin problems and prosthesis,” *Cutis*, vol. 55, no. 5, pp. 297–302, 1995.

[5] S. W. Levy, “Skin problems of the leg amputee,” *Prosthet. Orthot. Int.*, vol. 4, no. 1, pp. 37–44, Apr. 1980.

[6] N. L. Dudek, M. B. Marks, and S. C. Marshall, “Skin problems in an amputee clinic,” *Am. J. Phys. Med. Rehabil.*, vol. 85, no. 5, pp. 424–429, May 2006.

[7] H. E. J. Meulenbelt, J. H. B. Geertzen, P. U. Dijkstra, and M. F. Jonkman, “Skin problems in lower limb amputees: an overview by case reports,” *J. Eur. Acad. Dermatol. Venereol.*, vol. 21, no. 2, pp. 147–155, Feb. 2007.

[8] L. W. Lamoureux and C. W. Radcliffe, “Functional analysis of the UC-BL shank axial rotation device,” *Prosthet. Orthot. Int.*, vol. 1, no. 2, pp. 114–118, Aug. 1977.

[9] M. L. van der Linden, N. Twiste, and S. V. S. Rithalia, “The biomechanical effects of the inclusion of a torque absorber on trans- femoral amputee gait, a pilot study,” *Prosthet. Orthot. Int.*, vol. 26, no. 1, pp. 35–43, Jan. 2002.

[10] A. D. Segal, M. S. Orendurff, J. M. Czerniecki, J. B. Shofer, and G. K. Klute, “Transtibial amputee joint rotation moments during straight-line walking and a common turning task with and without a torsion adapter,” *J. Rehabil. Res. Dev.*, vol. 46, no. 3, pp. 375–383, 2009.

[11] B. C. Glaister, G. C. Bernatz, G. K. Klute, and M. S. Orendurff, “Video task analysis of turning during activities of daily living,” *Gait Posture*, vol. 25, no. 2, pp. 289–294, Feb. 2007.

[12] P.-F. Su, S. A. Gard, R. D. Lipshutz, and T. A. Kuiken, “The Effects of Increased Prosthetic Ankle Motions on the Gait of Persons with Bilateral Transtibial Amputations,” *Am. J. Phys. Med. Rehabil.*, vol. 89, no. 1, pp. 34–47, 2010.

[13] J. G. Buckley, S. F. Jones, and K. M. Birch, “Oxygen consumption during ambulation: Comparison of using a prosthesis fitted with and without a tele-torsion device,” *Arch. Phys. Med. Rehabil.*, vol. 83, no. 4, pp. 576–581, Apr. 2002.

[14] W. C. Miller, M. Speechley, and B. Deathe, “The prevalence and risk factors of falling and fear of falling among lower extremity amputees,” *Arch. Phys. Med. Rehabil.*, vol. 82, no. 8, pp. 1031–1037, Aug. 2001.

[15] A. D. Segal, M. S. Orendurff, J. M. Czerniecki, J. B. Shofer, and G. K. Klute, “Local dynamic stability in turning and straight-line gait,” *J. Biomech.*, vol. 41, no. 7, pp. 1486–93, Jan. 2008.

[16] A. D. Segal, M. S. Orendurff, J. M. Czerniecki, J. B. Shofer, and G. K. Klute, “Local dynamic stability of amputees wearing a torsion adapter compared to a rigid adapter during straight-line and turning gait,” *J. Biomech.*, vol. 43, no. 14, pp. 2798–803, Oct. 2010.

[17] B. C. Glaister, J. a Schoen, M. S. Orendurff, and G. K. Klute, “Mechanical behavior of the human ankle in the transverse plane while turning,” *IEEE Trans. Neural Syst. Rehabil. Eng.*, vol. 15, no. 4, pp. 552–559, Dec. 2007.

[18] K. Flick, M. Orendurff, J. Berge, A. Segal, and G. Klute, “Comparison of human turning gait with the mechanical performance of lower limb prosthetic transverse rotation adapters,” *Prosthet. Orthot. Int.*, vol. 29, no. 1, pp. 73–81, Jan. 2005.

[19] A. H. Hansen, D. S. Childress, S. C. Miff, S. a Gard, and K. P. Mesplay, “The human ankle during walking: implications for design of biomimetic ankle prostheses,” *J. Biomech.*, vol. 37, no. 10, pp. 1467–1474, Oct. 2004.

[20] A. Jafari, N. G. Tsagarakis, and D. G. Caldwell, “AwAS-II: A new Actuator with Adjustable Stiffness based on the novel principle of adaptable pivot point and variable lever ratio,” in *2011 IEEE International Conference on Robotics and Automation*, 2011, pp. 4638–4643.

[21] A. Jafari, N. G. Tsagarakis, I. Sardellitti, and D. G. Caldwell, “A New Actuator With Adjustable Stiffness Based on a Variable Ratio Lever Mechanism,” *IEEE/ASME Trans. Mechatronics*, vol. 19, no. 1, pp. 55–63, 2014.

[22] B. Kim, J. Park, and J. Song, “Double Actuator Unit with Planetary Gear Train for a Safe Manipulator,” in *2007 IEEE International Conference on Robotics and Automation*, 2007, pp. 1146–1151.

[23] M. Hutter, C. D. Remy, and R. Siegwart, “Design of an Articulated Robotic Leg With Nonlinear Series Elastic Actuation,” *Mob. Robot. - Solut. Challenges - Proc. Twelfth Int. Conf. Climbing Walk. Robot. Support Technol. Mob. Mach.*, pp. 645–652, 2010.

[24] C. Lagoda, A. C. Schouten, A. H. A. Stienen, E. E. G. Hekman, and H. Van Der Kooij, “Design of an electric Series Elastic Actuated Joint for robotic gait rehabilitation training,” in *International Conference on Biomedical Robotics and Biomechatronics*, 2010, pp. 21–26.

[25] B. C. Glaister, “Controllable Transverse Rotation Adaptor Patent,” US 2012/0153875 A12012.

[26] R. W. Selles, J. B. Bussmann, R. C. Wagenaar, and H. J. Stam, “Effects of prosthetic mass and mass distribution on kinematics and energetics of prosthetic gait: a systematic review,” *Arch. Phys. Med. Rehabil.*, vol. 80, no. 12, pp. 1593–9, Dec. 1999.

[27] J. Schuy, P. Beckerle, J. Wojtusch, S. Rinderknecht, and O. von Stryk, “Conception and evaluation of a novel variable torsion stiffness for biomechanical applications,” *2012 4th IEEE RAS EMBS Int. Conf. Biomed. Robot. Biomechatronics*, pp. 713–718, Jun. 2012.

[28] B. C. Glaister, J. a Schoen, M. S. Orendurff, and G. K. Klute, “A mechanical model of the human ankle in the transverse plane during straight walking: implications for prosthetic design,” *J. Biomech. Eng.*, vol. 131, no. 3, p. 034501, Mar. 2009.

[29] A. Jafari, N. G. Tsagarakis, and D. G. Caldwell, “A Novel Intrinsically Energy Efficient Actuator with Adjustable Stiffness (AwAS),” *IEEE/ASME Trans. Mechatronics*, vol. 18, no. 1, pp. 355–365, 2013.

[30] B.-S. Kim and J.-B. Song, “Hybrid dual actuator unit: A design of a variable stiffness actuator based on an adjustable moment arm mechanism,” in *ICRA 2010 IEEE International Conference on Robotics and Automation*, 2010, pp. 1655–1660.

[31] M. S. Orendurff, A. D. Segal, J. S. Berge, K. C. Flick, D. Spanier, and G. K. Klute, “The kinematics and kinetics of turning: limb asymmetries associated with walking a circular path,” *Gait Posture*, vol. 23, no. 1, pp. 106–111, Jan. 2006.

[32] E. Oberg, F. D. Jones, H. L. Horton, and H. H. Ryffel, *Machinery’s Handbook*, 29th ed. New York: Industrial Press, 2012, pp. 304–344, 2561–2564.

[33] R. C. Juvinall and K. M. Marshek, *Fundamentals of Machine Component Design*, 5th ed. New York: John Wiley & Sons, 2012, p. 411.

[34] D. A. Winter, *The Biomechanics and Motor Control of Human Gait: Normal, Elderly and Pathological*, 2nd ed. Waterloo: University of Waterloo Press, 1991, pp. 11–12.

[35] Maxon, “Data Sheet for Maxon EC 45 Motor,” 2014. [Online]. Available: http://www.maxonmotorusa.com/maxon/view/product/motor/ecmotor/ecflat/ecflat45/397172.

[36] M. J. D. Taylor, P. Dabnichki, and S. C. Strike, “A three-dimensional biomechanical comparison between turning strategies during the stance phase of walking,” *Hum. Mov. Sci.*, vol. 24, no. 4, pp. 558–73, Aug. 2005.

[37] S. A. England and K. P. Granata, “The influence of gait speed on local dynamic stability of walking,” *Gait Posture*, vol. 25, no. 2, pp. 172–178, 2007.

[38] V. Gremeaux, S. Damak, O. Troisgros, A. Feki, D. Laroche, D. Perennou, C. Benaim, and J.-M. Casillas, “Selecting a test for the clinical assessment of balance and walking capacity at the definitive fitting state after unilateral amputation: a comparative study.,” *Prosthet. Orthot. Int.*, vol. 36, no. 4, pp. 415–22, Dec. 2012.

[39] A. Deathe and W. Miller, “The L Test of Functional Mobility: Measurement Properties of a Modified Version of the Timed‘ Up & Go’ Test Designed for People With Lower-Limb Amputations,” *Phys. Ther.*, vol. 85, pp. 626–635, 2005.

[40] H. B. Menz, S. R. Lord, and R. C. Fitzpatrick, “Age-related differences in walking stability,” *Age Ageing*, vol. 32, no. 2, pp. 137–42, Mar. 2003.

[41] D. E. Krebs, D. Goldvasser, J. D. Lockert, G. Portney, and K. M. Gill-body, “Research Report Is Base of Support Greater in Unsteady Gait ?,” *Phys. Ther.*, vol. 82, pp. 138–147, 2002.

[42] P. Duncan, D. Weiner, J. Chandler, and S. Studenski, “Functional reach: A new clinical measure of balance,” *Journals Gerontol.*, vol. 45, no. 6, pp. M192–M197, 1990.